Multi-omics profiling, *in vitro* and *in vivo* enhancer assays dissect the *cis*-regulatory mechanisms underlying North Carolina macular dystrophy, a retinal enhanceropathy

Stijn Van de Sompele[1,2], Kent W. Small[3], Munevver Burcu Cicekdal[1,2,4], Víctor López Soriano[1,2], Eva D'haene[1,2], Fadi S. Shaya[3], Steven Agemy[5], Thijs Van der Snickt[1,2], Alfredo Dueñas Rey[1,2],Toon Rosseel[1,2], Mattias Van Heetvelde[1,2], Sarah Vergult[1,2], Irina Balikova[6], Arthur A. Bergen[7,8], Camiel J. F. Boon[9,10], Julie De Zaeytijd[11], Chris F. Inglehearn[12], Bohdan Kousal[13], Bart P. Leroy[2,11,14,15], Carlo Rivolta[16,17,18], Veronika Vaclavik[19], Jenneke van den Ende[20], Mary J. van Schooneveld[9,21], José Luis Gómez-Skarmeta[22], Juan J. Tena[22], Juan R. Martinez-Morales[22], Petra Liskova[13,23], Kris Vleminckx[2,4], Elfride De Baere[1,2]

1 Department of Biomolecular Medicine, Ghent University, Ghent, Belgium
2 Center for Medical Genetics, Ghent University Hospital, Ghent, Belgium
3 Macula and Retina Institute, Los Angeles and Glendale, California, USA
4 Department of Biomedical Molecular Biology, Ghent University, Ghent, Belgium
5 Department of Ophthalmology, SUNY Downstate Medical Center University, Brooklyn, New York, USA
6 Department of Ophthalmology, University Hospitals Leuven, Leuven, Belgium
7 Department of Human Genetics, Amsterdam UMC, Academic Medical Center, 1105 AZ Amsterdam, The Netherlands
8 Queen Emma Centre of Precision Medicine, Amsterdam University Medical Centre, University of Amsterdam, Amsterdam, The Netherlands
9 Department of Ophthalmology, Amsterdam University Medical Centers, University of Amsterdam, Amsterdam, The Netherlands
10 Department of Ophthalmology, Leiden University Medical Center, Leiden, The Netherlands
11 Department of Ophthalmology, Ghent University Hospital, Ghent, Belgium
12 Division of Molecular Medicine, Leeds Institute of Medical Research, University of Leeds, Leeds, UK
13 Department of Ophthalmology, First Faculty of Medicine, Charles University and General University Hospital in Prague, Prague, Czech Republic
14 Department of Head & Skin, Ghent University, Ghent, Belgium
15 Division of Ophthalmology & Center for Cellular & Molecular Therapeutics, Children's Hospital of Philadelphia, Philadelphia, PA, USA
16 Institute of Molecular and Clinical Ophthalmology Basel (IOB), Basel, Switzerland
17 Department of Ophthalmology, University of Basel, Basel, Switzerland
18 Department of Genetics and Genome Biology, University of Leicester, Leicester, UK
19 University of Lausanne, Jules-Gonin Eye Hospital, Lausanne, Switzerland
20 Center for Medical Genetics, Antwerp University Hospital, Antwerp, Belgium
21 Bartiméus, Diagnostic Center for Complex Visual Disorders, Zeist, The Netherlands

22 Centro Andaluz de Biología del Desarrollo, Consejo Superior de Investigaciones Científicas and Universidad Pablo de Olavide, Sevilla, Spain

23 Department of Paediatrics and Inherited Metabolic Disorders, First Faculty of Medicine, Charles University and General University Hospital in Prague, Prague, Czech Republic

Correspondence to:

Elfride De Baere, MD, PhD, Department of Biomolecular Medicine, Ghent University, Ghent, Belgium; Center for Medical Genetics, Ghent University Hospital, Ghent, Belgium. Email: elfride.debaere@ugent.be

Abstract

North Carolina macular dystrophy (NCMD) is a rare autosomal dominant disease affecting macular development. With the identification of non-coding single nucleotide variants (SNVs) near *PRDM13* and duplications overlapping a DNase I hypersensitive site (DHS) near *PRDM13* or *IRX1* as its underlying genetic cause, we hypothesize that NCMD is a retinal enhanceropathy. Here we aim to provide insight into the *cis*-regulatory mechanisms of NCMD by integrating multi-omics profiling of human retina with *in vitro* and *in vivo* enhancer assays.

First, we established RegRet (http://genome.ucsc.edu/s/stvdsomp/RegRet), a genome-wide multi-omics retinal database. Next, UMI-4C profiling was performed on adult human retina to fine-map chromatin interactions of *cis*-regulatory elements (CREs) with the *PRDM13* and *IRX1* promoters. Multi-omics analysis including the UMI-4C data revealed sixteen candidate CREs (cCREs), seven for the *PRDM13* and nine for the *IRX1* region. Subsequently, the activity of cCREs was investigated by *in vitro* luciferase assays and by *in vivo* enhancer assays in *Xenopus laevis* and *tropicalis*. Four cCREs showed *in vivo* eye- and brain-specific activity in *Xenopus*. Furthermore, we expanded the genetic architecture of NCMD with two novel non-coding SNVs (V15, V16) with a likely effect on *PRDM13* regulation. Luciferase assays showed that the non-coding SNVs that are located in the two hotspot regions of *PRDM13* have an effect on cCRE activity. Interestingly, cCRE4 in which V16 is located was shown to interact with the *PRDM13* promoter and demonstrated *in vivo* activity in *Xenopus*. This cCRE is active at a specific developmental stage (d103) compatible with the timepoint when retinal progenitor cells of the central retina exit mitosis. Mining of single-cell (sc) transcriptional data of embryonic and adult retina revealed the highest expression of *PRDM13* and *IRX1* when amacrine cells start to emerge and begin to synapse with retinal ganglion cells. This supports the hypothesis that altered *PRDM13* or *IRX1* expression impairs synaptic interactions between amacrine and ganglion cells during retinogenesis. Overall, this study gained insight into the *cis*-regulatory mechanisms of NCMD and supports that NCMD is a retinal enhanceropathy.

Keywords

North Carolina macular dystrophy (NCMD), *PRDM13*, *IRX1*, human retina, UMI-4C, multi-omics, *cis*-regulatory elements (CREs), single-cell (sc) RNA-seq, whole genome sequencing, non-coding single nucleotide variants (SNVs), duplications, enhancer assays, enhanceropathy

Introduction

The term "missing heritability", introduced by Brendan Maher in 2008, refers to the fact that the underlying genetic cause of many complex traits and diseases remains unexplained.[1] Although many technological advances in the field of genomics took place during the past decade, large-scale exome sequencing still has a limited diagnostic yield ranging from ~30-60%, depending on the condition being investigated.[2–4] It was estimated that 85% of mutations with large effects on disease-related traits can be identified in the protein-coding regions. Nevertheless, this number may result from the historical observational bias towards the approximately 1% coding part of the human genome, partly due to the fact that a significant portion of the non-coding genome still lacks proper functional annotation.[5] In the last couple of years, however, with the continuously reducing cost of next generation sequencing and the improvements of complementing analysis tools and algorithms, large-scale initiatives have contributed to the better understanding of the human genome and its different functional regions. According to the analysis of the Encyclopedia of DNA Elements (ENCODE) project, based on chromatin accessibility, transcriptional activity, and DNA methylation data, about 80% of the human genome may have a functional significance.[6] The majority of the identified functional elements, including gene promoters, enhancers, silencers, and insulators, appeared to be involved in controlling when and where genes located in the coding DNA are expressed. Control through these *cis*-regulatory elements (CREs) results from the presence of transcription factor binding sites (TFBS) for tissue- and time-specific transcription factors (TFs), which mediate the activation or repression of transcription.[7] It was also discovered that the human genome contains non-coding elements with an extremely high degree of sequence conservation across multiple vertebrate species. These are called ultra-conserved non-coding elements (UCNEs) and cluster in genomic regions associated with genes with a prior role during development.[8,9] Although studies in transgenic animals have shown that some of these elements function as tissue-specific enhancers during developmental processes, the functional significance of others remains to be ascertained.[10,11] To facilitate communication between CREs and target gene promoters, the genome is organized into well-defined three-dimensional domains, called topologically associating domains (TADs). This form of genome architecture, which is conserved across cell types, allows long-range interactions between CREs and their target genes within the same TAD, while insulating regulatory activity from neighboring TADs.[12] Whole genome sequencing (WGS) has revealed structural variants (SVs) that alter the copy number of CREs or disrupt TAD boundaries, resulting in modified 3D chromatin architecture.[13] Moreover, it has also been shown that single nucleotide variants (SNVs) residing in non-coding CREs could explain a certain fraction of the missing heritability, with the phenotypic consequences usually resulting from alterations in gene expression.[14–17] Thus far, an increasing number of non-coding variants have been linked to inherited retinal diseases (IRDs), the

majority of them affecting *cis*-acting splicing.[18–20] A well-known example is a deep-intronic mutation in *CEP290*, accounting for ~20% of congenital blindness due to Leber congenital amaurosis in Northwestern Europe.[21] In 2016, it was shown that North Carolina macular dystrophy (NCMD, MIM: 136550) is caused by non-coding SNVs near *PRDM13* and duplications overlapping with a DNase I hypersensitive site (DHS) near *PRDM13* or *IRX1*, likely dysregulating these TF-encoding genes.[22]

NCMD is a rare autosomal dominant disorder that affects the development of the macula as first noted by Small *et al.* [22–24] This completely penetrant maculopathy is present at birth, shows no progression, is characterized by variable expressivity (grade 1 to 3), even among family members, and usually affects both eyes symmetrically.[23,24] Grade 1 is characterized by a few small yellow drusen-like lesions within the fovea, which form larger confluent lesions in grade 2. In both grades, patients typically have no or mild impairment of central vision. In grade 3, the fundus has a striking appearance characterized by severe central colobomatous-like chorioretinal atrophy, resulting in mild to moderately impaired vision.[23,24] Although NCMD is generally considered as non-progressive, visual deterioration can be observed as a result of complications associated with choroidal neovascularization.[25] The disease was first described in 1971 upon the clinical investigation of a family from North Carolina,[26] and twenty years later, NCMD was mapped to chromosome 6q14-q16 (MCDR1 locus, MIM 136550).[27] During the following decades, linkage analysis was performed in many additional families giving a cumulative logarithm of the odds (LOD) score greater than 40.[28] Genetic heterogeneity was subsequently found with linkage to 5p15-p13 (MCDR3 locus, MIM 608850) in a single Danish family.[29] Since no mutations were found in the protein coding regions in both loci, Small *et al.* used WGS that eventually uncovered the first pathogenic non-coding variants underlying NCMD in 2016.[22] To date, eight heterozygous NCMD-associated tandem duplications have been reported. Five are located in the MCDR1 locus, encompassing the *PRDM13* gene and a shared non-coding region (~44 kb) upstream of the gene, containing several putative CREs.[22,30–33] The three tandem duplications located in the MCDR3 locus share a ~39 kb non-coding region in a gene desert downstream of the *IRX1* gene, while only one encompasses the coding region of *IRX1*.[22,25] Interestingly, the shared duplicated region in MCDR3 contains candidate CREs (cCREs) during retinal development as well as a UCNE of which the functions are yet unexplored.[8] In addition, six pathogenic heterozygous SNVs have been identified in the MCDR1 locus. They cluster together in two distinct hotspots, overlapping with cCREs upstream of the *PRDM13* gene.[22,34,35]

In this study, we aimed to provide insight into the *cis*-regulatory mechanisms of NCMD by integrated multi-omics profiling of human retina, *in silico* assessment, *in vitro* and *in vivo* enhancer assays of cCREs and (likely) pathogenic SNVs. Additionally, we expanded the mutational spectrum of NCMD by the identification of novel (likely) pathogenic SNVs in the *PRDM13* and *IRX1* regions.

Material and methods

Generation of an integrated retinal multi-omics database RegRet

In order to gain more insight into the regulatory landscapes of the two NCMD-associated disease loci, multiple tissue-specific datasets were collected and integrated into a genome-wide database. This database contains multiple ChIP-seq datasets of histone modifications and retinal TFs,[36] ATAC-seq data,[36,37] and RNA-seq data,[36,38], all generated in adult human retina. Moreover, DNase-seq data of embryonic retina at five different stages,[39] and Hi-C data from human retinal organoids were included.[40]

Tissue preparation and nuclei isolation

Rest material from two healthy human *post-mortem* cornea donors was obtained through the Tissue Bank of the Ghent University Hospital under ethical approval of the Ethics Committee of the Ghent University Hospital (2018/1072, B670201837286). Both donors (a 47- and 70-year-old male) did not have a history or clinical evidence of retinal disease. The eyes were transported in CO_2 Independent Medium (Gibco). Following dissection, retinas were processed according to the protocol of Matelot *et al.* (2016).[41] Briefly, retinas were treated with a 12.5% collagenase solution and forced through a 40 µm cell strainer, followed by crosslinking using a 2% formaldehyde solution. The crosslinking reaction was quenched by adding a cold 1 M glycine solution on ice. Cell suspensions were then centrifuged and washed with PBS. Cell lysis was performed using a 50 mM Tris-HCl, 150 mM NaCl, 5 mM EDTA, 0.5% NP-40, 1% Triton X-100 lysis buffer containing a complete protease inhibitor cocktail. Next, the lysates were centrifuged to obtain a pellet of nuclei. After a washing step with PBS, the nuclei were aliquoted per 10 million, snap frozen as a pellet in liquid nitrogen, and stored at -80°C. The maximum processing time between enucleation and preservation of nuclei was 24 h.

RNA isolation, cDNA conversion, qPCR

After retina dissection and before continuing with nuclei isolation, a small fraction of each of the collected retinal tissues was preserved in RNAlater (Qiagen). The tissues were thoroughly homogenized in the presence of TRIzol (Invitrogen). Next, total RNA was obtained through phenol-chloroform extraction. A DNase treatment was performed on-column using the RNeasy mini kit (Qiagen). The iScript cDNA synthesis kit (Bio-Rad) was used for RNA to cDNA conversion and subsequent qPCR analysis was performed using the SYBR Green Master Mix (Bio-Rad) and primers for retina-specific genes and controls. Expression values were analyzed in qbase+ (Biogazelle). Primer sequences can be found in Suppl. Table 1.

Generation of UMI-4C sequencing libraries

UMI-4C sequencing libraries were generated according to the protocol of Schwartzman *et al.* (2016).[42] For every library, the crosslinked DNA from 10 million nuclei was first digested overnight with 400 U *Dpn*II (NEB) at 37°C. Next, samples were diluted one in two before adding 4,000 U T4 DNA ligase (NEB) for overnight incubation at 16°C. Digestion and ligation efficiency were evaluated via agarose gel electrophoresis. DNA was then de-crosslinked with proteinase K (BIOzymTC). After overnight incubation at 65°C, the resulting 3C templates were purified using AMPure XP beads (Agencourt) and 4 µg of each template was sheared on a Covaris M220 focused-ultrasonicator (Covaris) to achieve 300 bp DNA fragments. The obtained fragments were library prepped using NEBNext Ultra II DNA Library Prep Kit (NEB) for Illumina. DNA shearing and library prep efficiency were evaluated on a Fragment Analyzer (Agilent Technologies). Next, a ligation-mediated nested PCR was conducted for every viewpoint of interest, using 100 ng of library as input, an upstream (US) forward primer, a universal reverse primer, and the KAPA2G Robust HotStart ReadyMix (Roche). After purification using AMPure XP beads (Agencourt), the resulting PCR product was used for the second PCR step, using a downstream (DS) forward primer and the same universal reverse primer. Primer sequences can be found in Suppl. Table 2. After purification, final library composition was evaluated on a Fragment Analyzer (Agilent Technologies).

UMI-4C sequencing and data-analysis

UMI-4C libraries were multiplexed in equimolar ratios and sequenced on the Illumina NovaSeq 6000 platform at 150 bp paired-end. Sequenced reads were demultiplexed based on their barcodes and their DS primer. UMI-4C data were then analyzed as described in Schwartzman *et al.* (2016) using the umi4cpackage in R (https://bitbucket.org/tanaylab/umi4cpackage).[42] Briefly, reads containing the primer sequence were first tested for a match with the pad sequence. Reads lacking this match were filtered out. After quality trimming, the restriction fragment ends, representing a potentially informative ligation partner, were mapped to the human genome using Bowtie2.[43] PCR duplicates were removed based on the UMI sequences, being the last ten bases of the 3' end of the read pair. Next, restriction fragment ends mapped to genomic coordinates within less than 1,500 bp of the viewpoint were considered as nondigested products and were excluded from the analysis. Contact intensity profiles around the viewpoint were constructed by extracting the number of ligations for all restriction fragment ends within a genomic window and pooling of this data from both samples. Finally, UMI-4C profiles were normalized and domainograms created.

Data mining in single-cell retinal dataset

Data generated by single-nucleus RNA-seq of embryonic (53, 59, 74, 78, 113, and 132 days) and adult (25, 50, and 54 years old) human retinal cells performed by Thomas *et al.* (2021) were processed for evaluating *PRDM13* and *IRX1* expression at single-cell level.[44] Expression matrices derived from nine *post-mortem* donor neural retinal samples (GSE183684) were imported into R (v4.0.5) and processed using the Seurat single-cell analysis package (v4.0).[45] Pre-processing and quality control was conducted to remove outlier cells. Briefly, we only considered genes with counts in at least three cells and filtered out cells that had unique feature (gene) counts <200 or >9,000 and that expressed >5% mitochondrial counts. The data were then total-count normalized, logarithmized, filtered for highly variable features, and scaled to unit variance. We used the Harmony package to merge all the single-cell data.[46] After quality control, pre-processing, and merging of all the data, a total of 60,014 retinal cells were kept for subsequent dimensionality reduction, embedding, and clustering. Markers associated with major neural retina cell populations were used to assess *IRX1* and *PRDM13* expression at single-cell level.

Targeted sequencing and qPCR

This study was approved by the ethics committee for Ghent University Hospital (2018/1566, B670201938572). The known NCMD-associated SNVs were analyzed on genomic DNA by PCR amplification of the two mutational hotspots, respectively containing the variants referenced as V1-V3, V12 and the V10-V11 variants, followed by Sanger sequencing using the BigDye Terminator v3.1 kit (Life Technologies). For detection of the previously reported tandem duplications, primers were designed specific for the duplication products. Fragment analysis was performed on a Fragment Analyzer (Agilent Technologies) using the PROSize 2.0 software. All primer sequences can be found in Suppl. Table 3. In the next step, copy number variant analysis was performed for a selection of regions implicated in the known tandem duplications. In particular, the copy number of the coding regions of *PRDM13* and *IRX1*, as well as the shared duplicated region downstream of *IRX1* were evaluated by qPCR using the SYBR Green Master Mix (Bio-Rad). Copy number values were analyzed in qbase+ (Biogazelle). All primer sequences can be found in Suppl. Table 3.

Whole genome sequencing (WGS)

Samples for WGS were prepared according to the Illumina TruSeq DNA PCR-free library preparation guide. The library of family F1 was sequenced on the Illumina HiSeq X-Ten platform at 350 bp paired-end, while all other libraries were sequenced on the Illumina NovaSeq 6000 platform at 150 bp paired-end. Reads were mapped to the human genome (hg38) using Isaac aligner (iSAAC-04.18.11.09)[47] and Strelka (2.9.10)[48] was used to identify SNVs and short indels. Variants were

annotated by SnpEff (v4.3t)[49] in combination with additional databases, including ESP6500,[50] ClinVar,[51] and dbNSFP3.5.[52] To identify SVs and large indels, the Manta (1.5.0)[53] software was utilized. At first, the two NCMD-associated disease loci were analyzed for candidate variants. Therefore, SNVs were filtered based on zygosity (heterozygous), Genome Aggregation Database (gnomAD v3.1.2)[54] population frequency (<0.005%), and genomic location (2 Mb and 4 Mb region around the *PRDM13* and *IRX1* gene, respectively corresponding to the TAD the gene is located in). SVs located in these genomic regions were evaluated using the Database of Genomic Variants (DGV, http://dgv.tcag.ca/dgv/app/home). Next, the coding regions of 275 known retinal disease genes (RetNet panel v5, https://sph.uth.edu/retnet/disease.htm) were assessed for (likely) pathogenic variants, both SNVs and SVs, that could explain a macular phenotype. Data analysis was performed using our in-house developed analysis platform Seqplorer, which incorporates gnomAD population frequencies, *in silico* missense predictions (REVEL, PolyPhen, SIFT, CADD, etc.), and splice predictions (MaxEntScan, SpliceRegion). Variants were confirmed by Sanger sequencing using the BigDye Terminator v3.1 kit (Life Technologies) and underwent segregation analysis where possible. All primer sequences can be found in Suppl. Table 3.

Clinical evaluation

Ophthalmic examination included fundus photography, optical coherence tomography (OCT), and measurement of best-corrected visual acuity (BCVA). In family F1, color vision was tested by means of a Lanthony D-15 saturated and desaturated assay.

In silico assessment of the non-coding SNVs in the mutational hotspots

For the previously reported and novel pathogenic NCMD-associated SNVs in the two mutational hotspots upstream of *PRDM13* (MHS1 and MHS2), potential effects of the nucleotide changes on TFBS motifs were analyzed using the TRANSFAC software.[55] Furthermore, an *in silico* assessment was performed using several functional prediction tools for human non-coding regulatory variants, including an integrated non-coding regulatory prediction score, regBase,[56] as well as several other tools (GenoCanyon,[57] ncER,[58] DVAR,[59] FIRE,[60] PAFA,[61] CDTS[62]).

In silico assessment of the NCMD-associated duplication breakpoints

A bioinformatics analysis was performed for the breakpoints of previously reported pathogenic NCMD-associated tandem duplications in the *PRDM13* and *IRX1* loci, as previously described.[63,64] In particular, the degree of microhomology (multiple sequence alignment, ClustalW), the presence of repetitive elements (RepeatMasker track UCSC Genome Browser), and the presence of sequence motifs, based

on 40 previously described motifs (Fuzznuc) were analyzed on the breakpoint regions of the tandem duplications.[65,66]

Generation of *in vitro* reporter constructs

Fourteen non-coding regions of interest were PCR amplified from human genomic DNA (Roche) using the Phusion High-Fidelity PCR Kit (NEB). Resulting products were cloned into the pGL4.23 luciferase reporter vector (Promega) by restriction-ligation cloning. The recombinant vectors were amplified in One Shot TOP10 Chemically Competent *E. coli* cells (Invitrogen) and purified using a QIAprep Spin Miniprep Kit (Qiagen). For the generation of the three reporter constructs containing duplicated regions of interest, a second round of restriction-ligation cloning was performed using different restriction enzymes. SNVs were inserted into the regions of interest using the Q5 Site-Directed Mutagenesis Kit (NEB) and mutation-specific primers were designed with the NEBaseChanger tool. The sequence of all inserts was confirmed by Sanger sequencing using the BigDye Terminator v3.1 kit (Life Technologies). All regions of interest, their respective primer sequences, and the mutagenesis primers can be found in Suppl. Table 4 & 5.

Cell culture

ARPE-19 cells (ATCC, CRL-2302) were grown in DMEM:F12 (Gibco, No. 30-2006) supplemented with 10% fetal bovine serum, 1% penicillin-streptomycin, 1% non-essential amino acid solution, and 0.1% amphotericin B. Cells were cultured at 37°C and 5% CO_2 and tested for mycoplasma contamination prior to use.

Luciferase enhancer assays

The recombinant pGL4.23 luciferase reporter vectors were transfected in equimolar amounts into ARPE-19 cells (ATCC, CRL-2302™) using the Lipofectamine 3000 Reagent Protocol, according to the manufacturer's instructions. The vectors were co-transfected with the pRL-TK *Renilla* luciferase control reporter vector (Promega) for normalization purposes. After 48h, cells were lysed and luciferase activity was detected using the Dual&Glo Luciferase Assay System (Promega) in a Glomax 96 Microplate Luminometer (Promega). Each transfection was done in triplicate and each experiment was repeated at least three times to ensure reproducibility. For each well, the ratio of firefly luciferase activity was normalized to *Renilla* luciferase activity. Next, these ratios were normalized to the average ratio of the corresponding control vector. For each SNV, the respective wild-type (WT) vector was used as a negative control, while the three vectors containing duplicated regions of interest were compared against their respective vectors containing the same region of interest as a single insert. For the set of

fourteen non-coding regions of interest, a vector containing an inactive insert of comparable length was used as a negative control. For each variant or region of interest, the effect on luciferase activity was determined using a linear mixed effects model in R, with the luciferase vector as fixed effect and the biological replicate as random effect. P-values were obtained by likelihood ratio tests of the model with the fixed effect against a null model without this effect.

Generation of *in vivo* reporter constructs

To functionally assess the potential *in vivo* activities of five non-coding regions of interest in the *PRDM13* and *IRX1* loci, SED vectors containing these regions were generated (Suppl. Table 6). Briefly, the regions of interest were PCR amplified from human genomic DNA (Roche) using *Taq* polymerase (Thermo Scientific) and cloned into the pCR-GW-TOPO vector (Invitrogen). Using LR Clonase II (Invitrogen), the DNA fragments were then subcloned into the destination SED vector. This *Xenopus* transgenesis compatible version of the fluorescent zebrafish enhancer detection (ZED)[67] vector utilizes a I-*Sce*I based detection system for assessing enhancer activity in *Xenopus* embryos.[68] A detailed description of the vector can be found in Suppl. Figure 1. Five non-coding regions with putative regulatory activity were inserted into a SED vector via Gateway cloning technology, as described previously.[69]

Functional characterization of cCREs using enhancer assays in *Xenopus* embryos

All experiments on *Xenopus tropicalis* and albino *Xenopus laevis* were executed in accordance with the guidelines and regulations of Ghent University, Faculty of Sciences, Belgium. Approval was obtained by the ethical committee of Ghent University, Faculty of Sciences, approval EC2014-089 and EC2017-104. For both WT *Xenopus tropicalis* and albino *Xenopus laevis*, females and males were primed with 20 U and 10 U human chorionic gonadotropin (hCG, Pregnyl, Merck), respectively. Natural mating was set-up the next day for *Xenopus tropicalis* and 5 days after priming for albino *Xenopus laevis*, after boosting the females and males with 150 and 100 U hCG, respectively. All the injections took place at the day of mating. Therefore, the I-*Sce*I meganuclease-mediated transgenesis protocol was followed, as described previously for *Xenopus*.[68] Briefly, a total of 100 ng of SED vector construct was digested with 5 U of I-*Sce*I meganuclease (NEB) at 37°C for 10 minutes in a 10 µL reaction mixture. Fertilized *Xenopus* eggs were obtained and dejellied using established protocols.[70] Embryos were then injected either unilaterally in the two-cell stage, or in two of the dorsal blastomeres at the four-cell stage, using 1 nL of the reaction mixture. Next, embryos were raised overnight at room temperature and replaced at 25.5°C for the rest of their development. Embryos were screened for EGFP reporter expression at different developmental stages using fluorescent microscopy.

Results

Establishment of RegRet, a genome-wide multi-omics retinal database

Multiple retinal datasets from different sources were integrated in a genome-wide multi-omics database. In particular, the database contains ChIP-seq datasets of histone modification H3K27ac from adult human retina, macula, and retinal pigment epithelium (RPE), and H3K4me2 from adult human retinal tissue.[36] Additional ChIP-seq datasets of retinal (CRX, NRL, OTX2, MEF2D, RORB) and other (CTCF, CREB) TFs, generated in adult human retina were included as well.[36] Next, we integrated available ATAC-seq data from both adult whole retina and macula,[36] as well as ATAC-seq data from adult retina and RPE, where a distinction was made between macular and peripheral regions.[37] In the context of retinal transcriptomics, quantitative RNA-seq data and newly identified transcripts observed in adult human retina were added,[38] in addition to single-nucleus RNA-seq data generated in adult human retina, macula, and RPE.[36] With regard to retina-specific chromatin interactions, Hi-C data from human retinal organoids was added.[40] To provide insight into retinal development, DNase-seq data from embryonic retinal tissue at five stages (74, 85, 89, 103, and 125 days) were included.[39] Apart from the retina-specific datasets, multiple non-retinal tracks were added: UCNEs and ultraconserved gene regulatory blocks (UGRBs),[8] H3K27Ac, H3K4Me1, and H3K4Me3 marks in seven cell lines (ENCODE Regulation), DHS peak clusters in 95 cell lines (ENCODE Regulation), ORegAnno elements,[71] ENCODE cCREs, RefSeq functional elements, GeneHancer regulatory elements and gene interactions, GeneCards gene transcription start sites, and Micro-C chromatin structure in H1-hESC. This genome-wide database, called RegRet (http://genome.ucsc.edu/s/stvdsomp/RegRet), is accessible via the UCSC Genome Browser and served as a basis for the subsequent locus-specific research of the NCMD-associated disease regions. Furthermore, it is also of use for studies of other retinal disease-associated loci.

UMI-4C profiling on human adult retina reveals cCREs of the *PRDM13* and *IRX1* regions

To identify the non-coding regions in the two known disease loci that interact with the *PRDM13* and *IRX1* promoters, we performed chromosome conformation capture, in particular UMI-4C, on retinas of adult human donor eyes. After dissection of the eyes, the purity of the retinal tissue was first demonstrated by expression analysis of several retina- and RPE-specific genes (Suppl. Figure 2). Next, UMI-4C was performed on the cross-linked retinal nuclei, using the *PRDM13* and *IRX1* promoter regions as bait sequences. The numbers of raw, mapped, and unique reads for each viewpoint can be found in Suppl. Table 7. For both genes, UMI-4C profiles indicated that promoter interactions were spread across but limited to their respective TAD (Figure 1). When these profiles were integrated into the retina-specific multi-omics database, based on overlap with peaks of epigenomics datasets, seven

and nine cCREs could be identified in the *PRDM13* and *IRX1* locus, respectively (Table 1 & Suppl. Figure 3).

One particularly interesting non-coding region was identified upstream of the *PRDM13* promoter (cCRE1). There, the UMI-4C data demonstrated a distinct interaction with the *PRDM13* promoter, in addition to an overlap with DNase-seq and ATAC-seq peaks, as well as with ChIP-seq profiles of specific histone marks indicative of enhancer activity (H3K27ac, H3K4me2) and ChIP-seq profiles of retinal TFs (CRX, NRL, OTX2). To confirm this interaction, a reverse UMI-4C experiment was conducted using this cCRE as a bait sequence. The resulting UMI-4C profile confirmed the interaction between the CRE and the *PRDM13* promoter, altogether making this region a very likely enhancer of *PRDM13* (Figure 2).

A second reverse UMI-4C experiment was performed for a non-coding region located ~800 kb downstream of the *IRX1* gene. This is the region of overlap of the three previously reported NCDM-associated tandem duplications in the *IRX1* locus (shared duplicated region, SDR) that also contains a UCNE (Figure 4). Although we were not able to identify an interaction using the *IRX1* promoter as a viewpoint, the reverse UMI-4C experiment suggested an interaction between the two regions (Suppl. Figure 4).

During retinal development *PRDM13* is predominantly expressed in amacrine cells and *IRX1* in retinal ganglion cells

Using the snRNA-seq data from six embryonic (53, 59, 74, 78, 113, and 132 days) and three adult (25, 50, and 54 years old) human retinal samples, we determined the expression pattern of *PRDM13* and *IRX1* during retinal development and in adult retina. The snRNA-seq data was first clustered into ten transcriptionally distinct clusters representing the major retinal cell types: amacrine cells, astrocytes, bipolar cells, cone photoreceptors, retinal ganglion cells, horizontal cells, microglia, Müller cells, retinal progenitor cells (RPCs), and rod photoreceptors (Figure 3A). To examine the dynamics of *PRDM13* and *IRX1* expression during retinal development, the different samples were then grouped into four time points: e50 = d53 and d59, e70 = d74 and d78, e100 = d113 and d132, adult = 3 samples. This revealed that throughout development *PRDM13* is predominantly expressed in amacrines cells, with some expression observed in RPCs, horizontal, and ganglion cells (Figure 3B & Suppl. Figure 5A). Compared to *PRDM13*, *IRX1* is generally lower expressed during development, with the highest expression in retinal ganglion cells and minimal expression in RPCs (Figure 3C & Suppl. Figure 5B). For both genes, the highest expression is observed at e70.

Novel non-coding SNVs found in the mutational hotspots of *PRDM13*

Twenty-three unrelated index cases with a clinical diagnosis of NCMD underwent targeted sequencing and copy number profiling of the known hotspots of the *PRDM13* and *IRX1* regions and WGS (subset of undiagnosed cases, n=9). A summary of the genetic findings can be found below and in Suppl. Table 8. An overview of the pedigrees and clinical details of the families with (likely) pathogenic variants can be found in Suppl. Figures 6 (F1), 7 (F2), and 8 (F3), and in Suppl. Table 8.

In the index case of a Czech family (F1-III:1), a novel heterozygous SNV was found in the second mutational hotspot (MHS2) of *PRDM13* (V15, chr6:99599064A>G), approximately 150 bp downstream of the previously reported V10 and V11 variants (Figure 4). Subsequent segregation analysis confirmed the variant in F1-III:1 and demonstrated the presence of this variant in the two affected daughters (F1-IV:1 and F1-IV:2) and the affected paternal aunt (F1-II:3). The variant was absent in the unaffected son of F1-II:3 (F1-III:5) (Suppl. Figure 6A). A second novel heterozygous SNV was identified in the index case from a Mexican family (F2-II:1). This SNV was found at the same nucleotide position as the previously reported V1 variant, albeit resulting in a different nucleotide change (V16, chr6:99593030G>C) (Figure 4). This variant, located in the first mutational hotspot (MHS1) of *PRDM13*, was present in three affected family members (F2-I:1, F2-III:1, and F2-III:2) and absent in three unaffected siblings (F2-II:2, F2-II:3, and F2-II:4). In the index case of another American family (F3-III:2), the known heterozygous V1 variant (chr6:99593030G>T) was identified, which was absent in two unaffected family members (F3-III:1 and F3-IV:1) and segregated in two affected family members (F3-II:1 and F3-II:3). All three reported variants are absent from gnomAD. In the other families, no potential (likely) pathogenic variants were identified in the two NCMD-associated disease loci or in the coding regions of 275 known retinal disease genes (RetNet panel v5).

Variable *in silico* predictions of SNVs associated with NCMD

Non-coding SNVs in the mutational hotspots (MHS) - Using TRANSFAC, the effect of the previously reported and novel NCMD-associated SNVs on TFBS was analyzed. This revealed that the novel SNV V15 (chr6:99599064A>G) is predicted to lead to the gain of an HSF1 TFBS, when compared to the WT sequence; while in case of the previously reported V10 variant (chr6:99598907A>C), the A to C nucleotide change results in a predicted loss of an POU2F1 (OCT1) TFBS (Suppl. Figure 9). For the six other known or novel SNVs, no effect on TFBS was observed.

The regBase_REG model, predicting the regulatory potential of a variant regardless of its functional direction and pathogenicity, generated relatively high scores for all variants in both hotspots. The regBase_PAT model on the other hand, which predicts the pathogenic capacity of a variant, scores the

variants in MHS1 as more likely to be pathogenic, compared to MHS2. According to GenoCanyon, which uses a cut-off of 0.5 to define functionality, the five variants located in MHS1 are all functional, having a score of 1.0. This is in contrast with the three variants in MHS2, which have low GenoCanyon scores. A similar result is obtained from the ncER prediction tool, which generates a score ranging from 0 (non-essential) to 100 (putative essential). There, the variants in the two hotspots have a score of ~70-80 and ~10-30, respectively. The DVAR scores, reflecting the probability of a variant being functional, are ~0.9 for variants in MHS1, and ~0.7 for variants in MHS2. The PHRED-scaled FIRE scores of all variants were comparable with those from DVAR, with higher scores suggesting greater capability to regulate nearby gene expression levels. Based on the PHRED-scaled PAFA scores, only variants V1 and V16 are predicted to have a functional effect. Finally, the CDTS scores demonstrate moderate intolerance to variation for all variants (Table 2).

Tandem duplications in the *PRDM13* and *IRX1* loci are caused by nonhomologous end-joining or replicative-based mechanisms

To assess the underlying mechanisms resulting in the eight previously reported NCMD-associated tandem duplications in the *PRDM13* and *IRX1* loci, bioinformatic analyses were performed on the breakpoint regions of these duplications. We found that three out of eight tandem duplication showed overlap with repetitive elements at both breakpoints. These pairs of elements, however, had little mutual sequence identity, since they were part of different classes. Apart from repetitive elements, other sequence motifs have also been shown to predispose to DNA breakage. Therefore, we investigated the 70 bp sequence surrounding the exact breakpoints of the eight tandem duplications for the presence of 40 sequence motifs previously associated with DNA breakage. Interestingly, one particular motif (deletion hotspot consensus, TGRRKM) was present in at least one breakpoint region of seven out of eight tandem duplications, while for four of these, this motif was present in both breakpoint regions. Moreover, the inclusion of several random nucleotides at the joint point (i.e. information scar) was observed at three tandem duplications, whereas a microhomology of two or three bps was present at six tandem duplications. Based on these results, we conclude that the tandem duplications are caused either by nonhomologous end-joining (NHEJ) or by a replicative-based mechanism, such as fork stalling and template switching (FoSTeS) or microhomology-mediated break-induced replication (MMBIR). In contrast to replicative-based mechanisms, NHEJ does not require microhomology, but is generally associated with the presence of an information scar (V4, V5, V6). Microhomology in the absence of an information scar in all other tandem duplications favors the hypothesis of a replicative-based mechanism. The sites of microhomology serve as priming location to invade the second replication fork after stalling or collapse of the first replication fork. For FoSTeS and

MMBIR, a single DNA break and the presence of microhomology at the breakpoints are sufficient to cause this template switching in a backward direction, which could have given rise to five out of eight tandem duplications (V7, V8, V9, V13, V14). A summary of these findings can be found in Suppl. Table 9, while the presence of microhomology is visualized in Suppl. Figure 10.

In vitro enhancer assays show a regulatory effect for non-coding SNVs of the *PRDM13* region

To determine the *in vitro* enhancer activity of a set of fourteen non-coding regions of interest, including the two MHSs, the SDR downstream of *IRX1*, and eleven other cCREs obtained after integrating the UMI-4C data into the retina-specific multi-omics database, these regions were cloned into separate luciferase reporter vectors (pGL4.23) (Suppl. Table 4). A negative control luciferase vector with an inactive insert of comparable length was used as reference. The subsequent luciferase assays in ARPE-19 cells demonstrated that seven of the tested regions were able to significantly increase luciferase reporter levels over the negative control vector ($P<0.001$), while two regions in the *IRX1* locus resulted in a decrease of luciferase expression ($P<0.001$). Remarkably, five regions, some of which had strong *in silico* predictions, did not show a significant difference in luciferase reporter levels compared to the negative control vector ($P>0.05$) (Suppl. Figure 11 & Suppl. Table 10).

Next, the potential effect of eight non-coding NCMD-associated SNVs on cCRE activity was assessed. Therefore, the two MHS-containing luciferase reporter vectors were subjected to site-directed mutagenesis to create eight individual variant vectors (Suppl. Table 5). The luciferase assays revealed that the four known variants in MHS1 (V1, V2, V3, V12) respectively resulted in a 2.6-, 2.8-, 1.6-, and 2.0-fold increase of reporter expression ($P<0.001$), relative to the WT vector (MHS1). Similar effects were obtained for the novel variant in the same region (V16). There, the relative luminescence was 3.2-fold higher ($P<0.001$) compared to the WT vector (MHS1) (Figure 5 & Suppl. Table 10). For the variants located in MHS2, an opposite trend was observed. The two known (V10, V11) and one novel variant (V15) in this region respectively demonstrated a 0.6-, 0.7-, and 0.6-fold decrease of luciferase expression ($P<0.001$), relative to the WT vector (MHS2) (Figure 5 & Suppl. Table 10).

The evaluate whether these non-coding regions of interest could have altered effects on reporter gene expression upon duplication, we analyzed luciferase activity of three regions located in the shared duplicated region of either the *PRDM13* or *IRX1* locus. Each of these regions was cloned into a separate luciferase reporter vector (pGL4.23) as a tandem duplication, to be compared against its reciprocal vector containing the same region as single insert. The results from the luciferase assays show that in case of all three cCREs, a 0.5-fold decrease in expression levels of the luciferase reporter ($P<0.001$) is exhibited by the duplicated region in comparison with its single region counterpart (Figure 5 & Suppl. Table 10).

In vivo enhancer assays in *Xenopus* display eye- and brain-specific activity for four cCREs from the *PRDM13* and *IRX1* loci

In order to address the activity of cCREs *in vivo*, five non-coding regions of interest were cloned into the SED vector, upstream of a minimal *gata2* promoter element and an EGFP reporter gene. In particular, the two MHSs and the cCRE with the strongest epigenomic signatures (cCRE1) from the *PRDM13* locus were selected, as well as the SDR and the cCRE with the highest *in vitro* activity (cCRE14) from *IRX1* locus. All constructs were injected unilaterally in two-cell stage *Xenopus tropicalis* embryos, the non-injected side of which acted as an internal negative control. In line with the *irx1* expression in the neural plate in neurula stages of *Xenopus* embryos, the cCRE14 construct drove EGFP reporter expression in neural plate and tube in the injected side of the embryos at Nieuwkoop and Faber (NF) stage 15 and 20 (Figure 6A & 6B).[72] At NF stage 42/43 and 45, EGFP reporter expression was detected in the craniofacial cartilage, a derivative of the neural crest (NC), and in the eye (Figure 6C & 6D). In these transgenic tadpoles, DsRed expression, which in the SED vector is driven by the *Xenopus* cardiac actin promoter, was visible in muscles, thereby demonstrating successful transgene integration (Figure 6E & 6F). When the tadpoles were grown and screened for EGFP reporter expression before metamorphosis at NF stage 55, 13 out of 30 transgenic embryos were found to express EGFP in the eye of the injected side, which was visible through the lens of the dark-pigmented eye (Figure 6G). Meanwhile, no EGFP reporter expression was observed in the eye on the non-injected side of these tadpoles (Figure 6H). The findings from the other *Xenopus tropicalis* transgenesis experiments are summarized in Suppl. Table 11.

As EGFP reporter expression driven by the SED vector reporter constructs becomes obscured by the pigmentation of the eyes in the tadpole stages, albino *Xenopus laevis* animals were used to obtain embryos with non- or poorly-pigmented eyes. Transgenic albino embryos that were unilaterally injected with the cCRE14 reporter construct in the two-cell stage demonstrated EGFP reporter expression in the eye and the brain in 10 out of 14 tadpoles at NF stage 42/43 (Figure 6I & 6J), in line with the findings in *Xenopus tropicalis.* When the reporter construct was introduced in the dorsal blastomeres at the four-cell stage, EGFP reporter expression in the eye and brain was observed in 17 out of 19 transgenic tadpoles (Figure 6K & 6L). The SED vector reporter construct containing the SDR of the *IRX1* locus also demonstrated comparable EGFP reporter expression, albeit with a much lower intensity (Figure 6M & 6N). Regarding the non-coding regions of interest of the *PRDM13* locus, the reporter construct containing the first mutational hotspot (MHS1) region did not drive any EGFP reporter expression in the transgenic embryos at NF stage 42/43 (Figure 6R), while EGFP reporter expression in the eye and brain was observed for the second mutational hotspot (MHS2, cCRE4) region (Figure 6S & 6T) and cCRE1 (Figure 6U & 6V). This is in line with previous findings of *in situ* hybridization

in *Xenopus laevis* embryos, demonstrating that *prdm13* expression is observed in progenitor cells of the developing retina, from NF stage 28 onwards. At NF stage 42/43, *prdm13* is detected in the amacrine cells, located in the inner part for the inner nuclear layer.[73,74] A summary of the findings of the *Xenopus laevis* transgenesis experiments is given in Suppl. Table 11.

Discussion

In the last decade, it became evident that non-coding variants contribute significantly to the molecular pathogenesis of IRDs. Although an increasing number of pathogenic variants affecting *cis*-acting splicing have been identified,[18–20] variants located in non-coding *cis*-acting regulatory elements are scarcer.[75–77] The identification and interpretation of the latter, however, remains challenging as the exact mechanisms of the elements they are located in, the genes they act on, and the effect of the variation remains largely unknown. Here, we have focused on NCMD, a developmental macular disorder caused by non-coding SNVs and tandem duplications assumed to affect *PRDM13* (MCDR1 locus) and *IRX1* (MCDR3 locus) expression.

The establishment of RegRet, a genome-wide multi-omics retinal database, advances genome annotation in human retina. It not only laid the foundation for the locus-specific research of the two genomic regions implicated in NCMD, but also represents a universal framework for studies of other loci implicated in rare IRDs as well as complex retinal diseases.

By integrating chromosome conformation capture (UMI-4C) profiles for the *PRDM13* and *IRX1* promoter, generated on adult human retinal tissue, with multiple genome-wide retinal datasets on DNA accessibility, epigenetic histone marks, TF binding, and gene expression, we were able to both characterize cCREs and determine which of these physically interact with the two promoters of interest, revealing seven and nine cCRE-gene connections, respectively. Although *in vitro* luciferase assays did not demonstrate regulatory activity for all of these regions, *in vivo* experiments in *Xenopus* embryos could confirm eye- and brain-specific activity for three of the most promising cCREs in both the *PRDM13* (cCRE1, cCRE4) and *IRX1* locus (cCRE14), as well as for the shared duplicated region downstream of *IRX1* (SDR), containing a UCNE. Moreover, the interaction of cCRE1 with the *PRDM13* promoter was confirmed by a reverse UMI-4C experiment, on top of appropriate DNA accessibility and ChIP-seq data, putting forward this region as a novel enhancer of *PRDM13*. The *PRDM13* (PR/SET Domain 13) gene encodes a TF characterized by an N-terminal PR domain with histone methyltransferase activity, followed by four zinc-finger domains, responsible for protein-protein and protein-DNA binding. During embryogenesis, the TF has been characterized as a transcriptional repressor responsible for ventral cell type specification in the dorsal neural tube.[78] In the retina, PRDM13 also acts as a cell type specification factor. In particular, while the TF PTF1A plays a key role in amacrine and horizontal cell fate specification, its downstream target PRDM13 is essential for the development and diversification of specific subsets of amacrine cells. Based on their morphological, neurochemical, and physiological features, more than 30 subtypes of amacrine cells can be defined, each having a distinct set of functions. Most PRDM13-positive amacrine cells use GABA or glycine as a neurotransmitter and adapt visual sensitivity to changing contrast and spatiotemporal frequency. As a

consequence, *Prdm13* knockout significantly reduces this amacrine cell subtype.[79] Using single-cell transcriptional mining, we indeed showed that *PRDM13* is expressed in the fetal retina, with the highest values in the amacrine cells between d74 and d78, while little to no expression is observed in adult retinal neurons. Since we performed the UMI-4C experiments on adult human retinas, this could explain why the first mutational hotspot, which is expected to have a role during retinal development, did not show an interaction with the *PRDM13* promoter. Indeed, using the activity-by-contact (ABC) method based on Hi-C data from human embryonic stem cells, Green *et al.* (2021) demonstrated that both hotspots encompass cCREs.[80] Interestingly, 70% of the macula-specific CREs that were identified in this study correspond with the seven candidate CREs that we identified in the *PRDM13* locus (Suppl. Figure 12). It should also be noted that the quality of UMI-4C profiles, reflected by the number of UMIs, is dependent on both the genomic region the viewpoint is located in and the efficiency of the nested PCR reactions. The same holds true for the reverse UMI-4C experiment on adult retinal tissue using the shared duplicated region, located ~800kb downstream from the *IRX1* promoter, as a bait. The obtained profile hinted at an interaction between this region and the *IRX1* promoter, while the promoter-based UMI-4C experiment did not. Similar to *PRDM13*, analysis of scRNA-seq data illustrated absence of *IRX1* expression in adult retinal tissue, while highest expression was shown between d74 and d78 in retinal ganglion cells.

Genomic profiling of 23 index cases with a clinical diagnosis of NCMD revealed two novel non-coding SNVs. Variant V15 (chr6:99599064A>G), located in the second mutational hotspot of the *PRDM13* region, and segregating in three affected family members, is absent from gnomAD and has varying predictions of functionality and pathogenicity. This could be explained by the fact that most prediction tools are based on supervised modeling, and therefore heavily rely on the composition and annotation of the training dataset used, which might not sufficiently represent the type of variants under investigation. However, the nucleotide change of variant V15 causes a predicted gain of an HSF1 TFBS. For the V10 variant, located in the same hotspot, a similar effect was observed, albeit resulting in the loss of a POU2F1 (OCT1) TFBS. Interestingly, for both HSF1 and POU2F1, activity in the neuroretina has been demonstrated.[81,82] The second novel variant, variant V16 (chr6:99593030G>C), is located in the first mutational hotspot of the *PRDM13* region and constitutes a different nucleotide change at the same nucleotide position as the previously reported V1 variant.[22] For these and the three other variants in the first hotspot, *in silico* predictions support a variant effect. When comparing both the novel and previously reported SNVs against their WT sequences using luciferase assays in ARPE-19 cells, we showed that all SNVs exert an effect on reporter gene expression. In case of the first hotspot, the five variants had an increased activity, with the novel V16 variant having the strongest effect, whereas the three variants in the second hotspot all demonstrated a decreased activity. Both hotspots

have been identified as cCREs active at d103 of embryonic development, i.e. the moment when retinal progenitor cells of the macula exit mitosis and differentiate towards photoreceptor fate, [80,83] and the luciferase assays show an effect of the SNVs they contain on reporter gene expression. Therefore, impairment of *PRDM13* expression during a critical step of maculogenesis can be assumed. Indeed, *Prdm13* knockout in mice and overexpression of the *PRDM13* orthologue in *Drosophila* (CG13296) presented with abnormal retinal and eye development, respectively.[31,79] Apart from non-coding SNVs, five NCMD-associated tandem duplications have also been identified in the *PRDM13* locus. These have a ~44kb shared duplicated region which comprises four cCREs we identified and both mutational hotspots. Based on luciferase assays, we demonstrated that the duplication of two of these regions (MHS1, cCRE1) also affects reporter gene expression. In addition, this region contains a CTCF binding site, indicative of a sub-TAD boundary, as determined using the RegRet database. A duplication thereof could thus lead to the generation of a neo-TAD, associated with gain-of-function effects of certain CREs, resulting in altered target gene expression.[13,84]

Most vertebrate species possess six Iroquois (*IRX*) genes, located in two paralog clusters. These genes encode important developmental homeobox TFs, with key roles in regulating gene expression during pattern formation and nervous system development.[85,86] More specifically, in mice all six *Irx* genes are expressed in the inner layers of the neuroretina during early retinogenesis and *Irx1* is required for the neurogenesis of the inner and outer nuclear layer of the retina. The latter has been also demonstrated in zebrafish, where *irx1a* knockdown negatively affects the proper differentiation of amacrine, bipolar, photoreceptor, and Müller glial cells.[87,88] Since only one of the three previously reported NCMD-associated tandem duplications in the *IRX1* locus and at least four benign duplications from DGV span the coding region of the *IRX1* gene, we can assume that the disease-causing mechanisms associated with these duplications do not result from impaired *IRX1* dosage itself, but have a regulatory basis. In the ~39kb shared duplicated region downstream of *IRX1*, we identified a UCNE which is, based on DNase-seq data from the developing retina, active between d85 and d103 of development. Similar to the observations in the hotspots of the *PRDM13* locus, this period corresponds to an important moment in human maculogenesis, characterized by the proliferation and differentiation of retinal progenitor cells.[83] *In vivo Xenopus* experiments demonstrated eye-specific and developmental activity of this UCNE-containing region, and the duplication was shown to have an effect on luciferase reporter expression *in vitro*.

By single-cell RNA sequencing of different macular subregions, Voigt *et al.* (2021) demonstrated region-specific gene expression and alternative splicing.[89] Although this unique character of the human macula and its development are not fully represented by *in vitro* studies in postnatal cells and *in vivo* assays in a model organism lacking a macula, we have provided evidence that NCMD-associated

variants can affect *PRDM13* and *IRX1* expression, due to nucleotide changes in regulatory sequences, gene duplication, the duplication of one or more CREs, or the disturbance of the gene regulatory landscape. Based on these findings, we put forward a hypothesis on how transcriptional changes in two distinct loci can result in the same macular phenotype. In particular, by transcriptome profiling based on RNA-seq data from thirteen human fetal retina samples spanning different developmental stages, Hoshino *et al.* (2017) revealed three key epochs in the transcriptional dynamics of human retina between d52 and d150.[90] Our analysis of single-cell RNA-seq data of embryonic retina illustrated that both *PRDM13* and *IRX1* demonstrate their highest expression at the beginning of epoch two (d67 to d80), corresponding to the moment when amacrine cells start to emerge and begin to synapse with retinal ganglion cells.[90] We therefore hypothesize that altered *PRDM13* or *IRX1* expression impairs macula-specific synaptic interactions between amacrine and ganglion cells during retinogenesis. In future studies, transcriptome and chromatin interaction studies on patient-derived retinal organoids may be useful to evaluate the effect of SNVs and tandem duplications on gene expression, genome organization, and cellular differentiation and function *in vivo.*

In conclusion, we have provided an integrated retinal multi-omics database, which advances the annotation of the genome in human retina and represents a universal framework for disease-associated loci implicated in rare as well as complex retinal diseases. By integrated multi-omics profiling of human retina, and by an in-depth *in silico*, *in vitro* and *in vivo* assessment of cCREs and variants therein, we have gained insight into the *cis*-regulatory mechanisms and genetic architecture of NCMD. Overall, this supports the hypothesis that NCMD is a retinal enhanceropathy, which is unique in the wider group of IRDs. With a broader implementation of WGS in rare disease research, an emphasis shift to non-coding regions such as CREs as targets of mutations can be expected. Finally, our study is exemplar for how expanding knowledge of disease-causing mechanisms and phenotype-driven genomic and functional data profiling of non-coding regions, advance our ability to fully interpret variants in non-coding regions in rare diseases. Providing a definitive genetic diagnosis in more individuals with rare diseases is imperative for the design of efficient disease-specific genetic testing, genetic counseling, and ultimately for therapeutic decisions.

References

1. Maher, B. Personal genomes, the case of the missing heritability. *Nature* **456**, 18–21 (2008).

2. Farwell, K. D. *et al.* Enhanced utility of family-centered diagnostic exome sequencing with inheritance model-based analysis: Results from 500 unselected families with undiagnosed genetic conditions. *Genetics in Medicine* **17**, 578–586 (2015).

3. Haer-Wigman, L. *et al.* Diagnostic exome sequencing in 266 Dutch patients with visual impairment. *European Journal of Human Genetics* **25**, 591–599 (2017).

4. Arts, P. *et al.* Exome sequencing in routine diagnostics: A generic test for 254 patients with primary immunodeficiencies. *Genome Medicine* **11**, (2019).

5. Majewski, J., Schwartzentruber, J., Lalonde, E., Montpetit, A. & Jabado, N. What can exome sequencing do for you? *Journal of Medical Genetics* vol. 48 580–589 (2011).

6. Dunham, I. *et al.* An integrated encyclopedia of DNA elements in the human genome. *Nature* **489**, 57–74 (2012).

7. Khurana, E. *et al.* Role of non-coding sequence variants in cancer. *Nature Reviews Genetics* vol. 17 93–108 (2016).

8. Dimitrieva, S. & Bucher, P. UCNEbase - A database of ultraconserved non-coding elements and genomic regulatory blocks. *Nucleic Acids Research* **41**, 101–109 (2013).

9. Harmston, N., Barešić, A. & Lenhard, B. The mystery of extreme non-coding conservation. *Philosophical Transactions of the Royal Society B: Biological Sciences* **368**, (2013).

10. de La Calle-Mustienes, E. *et al.* A functional survey of the enhancer activity of conserved non-coding sequences from vertebrate Iroquois cluster gene deserts. *Genome Research* **15**, 1061–1072 (2005).

11. Pennacchio, L. A. *et al.* In Vivo Enhancer Analysis of Human Conserved Noncoding Sequences. *Nature* **444**, 499–502 (2006).

12. Dixon, J. R. *et al.* Topological domains in mammalian genomes identified by analysis of chromatin interactions. *Nature* **485**, 376–380 (2012).

13. Spielmann, M., Lupiáñez, D. G. & Mundlos, S. Structural variation in the 3D genome. *Nature Reviews Genetics* **19**, 453–467 (2018).

14. Hoang, P. H. *et al.* Whole-genome sequencing of multiple myeloma reveals oncogenic pathways are targeted somatically through multiple mechanisms. *Leukemia* **32**, 2459–2470 (2018).

15. Carss, K. *et al.* Comprehensive Rare Variant Analysis via Whole-Genome Sequencing to Determine the Molecular Pathology of Inherited Retinal Disease. *American Journal of Human Genetics* **100**, 75–90 (2017).

16. Guo, C. *et al.* Coordinated regulatory variation associated with gestational hyperglycaemia regulates expression of the novel hexokinase HKDC1. *Nature Communications* **6**, 6096 (2015).

17. van den Boogaard, M. *et al.* A common genetic variant within SCN10A modulates cardiac SCN5A expression. *Journal of Clinical Investigation* **124**, 1844–1852 (2014).

18. Weisschuh, N. *et al.* Deep-intronic variants in CNGB3 cause achromatopsia by pseudoexon activation. *Human Mutation* **41**, 255–264 (2020).

19. Khan, M. *et al.* Resolving the dark matter of ABCA4 for 1054 Stargardt disease probands through integrated genomics and transcriptomics. *Genetics in Medicine* **22**, 1235–1246 (2020).

20. Qian, X. *et al.* Identification of Deep-Intronic Splice Mutations in a Large Cohort of Patients With Inherited Retinal Diseases. *Frontiers in Genetics* **12**, (2021).

21. den Hollander, A. I. *et al.* Mutations in the CEP290 (NPHP6) Gene Are a Frequent Cause of Leber Congenital Amaurosis. *The American Journal of Human Genetics* **79**, 556–561 (2006).

22. Small, K. W. *et al.* North Carolina Macular Dystrophy Is Caused by Dysregulation of the Retinal Transcription Factor PRDM13. *Ophthalmology* **123**, 9–18 (2016).

23. Small, K. W. North Carolina Macular Dystrophy, Revisited. *Ophthalmology* **96**, 1747–1754 (1989).

24. Small, K. W. *et al.* North Carolina Macular Dystrophy Is Assigned to Chromosome 6. *Genomics* **13**, 681–685 (1992).

25. Cipriani, V. *et al.* Duplication events downstream of IRX1 cause North Carolina macular dystrophy at the MCDR3 locus. *Scientific Reports* **7**, (2017).

26. Lefler, W. H., Wadsworth, J. A. C. & Sidbury, J. B. Hereditary macular degeneration and amino-aciduria. *American Journal of Ophthalmology* **71**, 224–230 (1971).

27. Small, K. W., Weber, J., Roses, A. & Pericak-Vance, P. North Carolina macular dystrophy (MCDR1): A review and refined mapping to 6q14-q16.2. *Ophthalmic Paediatrics and Genetics* **14**, 143–150 (1993).

28. Small, K. W. North Carolina macular dystrophy: clinical features, genealogy, and genetic linkage analysis. *Trans Am Ophthalmol Soc* **96**, 925–961 (1998).

29. Rosenberg, T. *et al.* Clinical and genetic characterization of a Danish family with North Carolina macular dystrophy. *Molecular Vision* **16**, 2659–2668 (2010).

30. Bowne, S. J. *et al.* North Carolina macular dystrophy (MCDR1) caused by a novel tandem duplication of the PRDM13 gene. *Molecular Vision* **22**, 1239–1247 (2016).

31. Manes, G. *et al.* A novel duplication of PRMD13 causes North Carolina macular dystrophy: Overexpression of PRDM13 orthologue in drosophila eye reproduces the human phenotype. *Human Molecular Genetics* **26**, 4367–4374 (2017).

32. Wu, S. *et al.* A novel tandem duplication of PRDM13 in a Chinese family with North Carolina macular dystrophy. *Graefe's Archive for Clinical and Experimental Ophthalmology* (2021) doi:10.1007/s00417-021-05376-w.

33. Small, K. W. *et al.* A novel duplication involving PR DM13 in a Turkish family supports its role in North Carolina macular dystrophy (NCMD/MCDR1). *Molecular Vision* **27**, 518–527 (2021).

34. Silva, R. S. *et al.* Unique non-coding variants upstream of PRDM13 are associated with a spectrum of developmental retinal dystrophies including Progressive Bifocal Chorioretinal Atrophy. *Human Mutation* **40**, 578–587 (2019).

35. Namburi, P. *et al.* A unique PRDM13-associated variant in a Georgian Jewish family with probable North Carolina macular dystrophy and the possible contribution of a unique CFH variant. *Molecular Vision* **26**, 299–310 (2020).

36. Cherry, T. J. *et al.* Mapping the cis-regulatory architecture of the human retina reveals noncoding genetic variation in disease. *PNAS* **117**, 9001–9012 (2020).

37. Wang, J. *et al.* ATAC-Seq analysis reveals a widespread decrease of chromatin accessibility in age-related macular degeneration. *Nature Communications* **9**, 1364 (2018).

38. Pinelli, M. *et al.* An atlas of gene expression and gene co-regulation in the human retina. *Nucleic Acids Research* **44**, 5773–5784 (2016).

39. Meuleman, W. *et al.* Index and biological spectrum of human DNase I hypersensitive sites. *Nature* **584**, 244–251 (2020).

40. de Bruijn, S. E. *et al.* Structural Variants Create New Topological-Associated Domains and Ectopic Retinal Enhancer-Gene Contact in Dominant Retinitis Pigmentosa. *American Journal of Human Genetics* **107**, 802–814 (2020).

41. Matelot, M. & Noordermeer, D. Determination of high-resolution 3D chromatin organization using circular chromosome conformation capture (4C-seq). *Methods in Molecular Biology* **1480**, 223–241 (2016).

42. Schwartzman, O. *et al.* UMI-4C for quantitative and targeted chromosomal contact profiling. *Nature Methods* **13**, 685–691 (2016).

43. Langmead, B. & Salzberg, S. L. Fast gapped-read alignment with Bowtie 2. *Nature Methods* **9**, 357–359 (2012).

44. Thomas, E. D. *et al.* Multi-omic Analysis of Developing Human Retina and Organoids Reveals Cell-Specific Cis-Regulatory Elements and Mechanisms of Non-Coding Genetic Disease Risk. *bioRxiv* (2021) doi:10.1101/2021.07.31.454254.

45. Hao, Y. *et al.* Integrated analysis of multimodal single-cell data. *Cell* **184**, 3573–3587 (2021).

46. Korsunsky, I. *et al.* Fast, sensitive and accurate integration of single-cell data with Harmony. *Nature Methods* **16**, 1289–1296 (2019).

47. Raczy, C. *et al.* Isaac: Ultra-fast whole-genome secondary analysis on Illumina sequencing platforms. *Bioinformatics* **29**, 2041–2043 (2013).

48. Kim, S. *et al.* Strelka2: fast and accurate calling of germline and somatic variants. *Nature Methods* **15**, 591–594 (2018).

49. Cingolani, P. *et al.* A program for annotating and predicting the effects of single nucleotide polymorphisms, SnpEff: SNPs in the genome of Drosophila melanogaster strain w1118; iso-2; iso-3. *Fly* **6**, 80–92 (2012).

50. NHLBI GO Exome Sequencing Project (ESP). Exome Variant Server. http://evs.gs.washington.edu/EVS/ (2019).

51. Landrum, M. J. *et al.* ClinVar: Improving access to variant interpretations and supporting evidence. *Nucleic Acids Research* **46**, D1062–D1067 (2018).

52. Liu, X., Wu, C., Li, C. & Boerwinkle, E. dbNSFP v3.0: A One-Stop Database of Functional Predictions and Annotations for Human Nonsynonymous and Splice-Site SNVs. *Human Mutation* **37**, 235–241 (2016).

53. Chen, X. *et al.* Manta: Rapid detection of structural variants and indels for germline and cancer sequencing applications. *Bioinformatics* **32**, 1220–1222 (2016).

54. Karczewski, K. J. *et al.* The mutational constraint spectrum quantified from variation in 141,456 humans. *Nature* **581**, 434–443 (2020).

55. Wingender, E. The TRANSFAC project as an example of framework technology that supports the analysis of genomic regulation. *Briefings in Bioinformatics* **9**, 326–332 (2008).

56. Zhang, S. *et al.* regBase: whole genome base-wise aggregation and functional prediction for human non-coding regulatory variants. *Nucleic Acids Research* **47**, e134 (2019).

57. Lu, Q. *et al.* A statistical framework to predict functional non-coding regions in the human genome through integrated analysis of annotation data. *Scientific Reports* **5**, 10576 (2015).

58. Wells, A. *et al.* Ranking of non-coding pathogenic variants and putative essential regions of the human genome. *Nature Communications* **10**, 5241 (2019).

59. Yang, H. *et al.* De novo pattern discovery enables robust assessment of functional consequences of non-coding variants. *Bioinformatics* **35**, 1453–1460 (2019).

60. Ioannidis, N. M. *et al.* FIRE: Functional inference of genetic variants that regulate gene expression. *Bioinformatics* **33**, 3895–3901 (2017).

61. Zhou, L. & Zhao, F. Prioritization and functional assessment of noncoding variants associated with complex diseases. *Genome Medicine* **10**, 53 (2018).

62. di Iulio, J. *et al.* The human noncoding genome defined by genetic diversity. *Nature Genetics* **50**, 333–337 (2018).

63. Verdin, H. *et al.* Microhomology-Mediated Mechanisms Underlie Non-Recurrent Disease-Causing Microdeletions of the FOXL2 Gene or Its Regulatory Domain. *PLoS Genetics* **9**, (2013).

64. Vissers, L. E. L. M. *et al.* Rare pathogenic microdeletions and tandem duplications are microhomology-mediated and stimulated by local genomic architecture. *Human Molecular Genetics* **18**, 3579–3593 (2009).

65. Rice, P., Longden, I. & Bleasby, A. EMBOSS: the European Molecular Biology Open Software Suite. *Trends in Genetics* **16**, 276–277 (2000).

66. Abeysinghe, S. S., Chuzhanova, N., Krawczak, M., Ball, E. v. & Cooper, D. N. Translocation and gross deletion breakpoints in human inherited disease and cancer I: Nucleotide composition and recombination-associated motifs. *Human Mutation* **22**, 229–244 (2003).

67. Bessa, J. *et al.* Zebrafish Enhancer Detection (ZED) vector: A new tool to facilitate transgenesis and the functional analysis of cis-regulatory regions in zebrafish. *Developmental Dynamics* **238**, 2409–2417 (2009).

68. Ogino, H., McConnell, W. B. & Grainger, R. M. High-throughput transgenesis in Xenopus using I-SceI meganuclease. *Nature Protocols* **1**, 1703–1710 (2006).

69. Bessa, J. & Gómez-Skarmeta, J. L. Making Reporter Gene Constructs to Analyze Cis-regulatory Elements. in *Molecular Methods for Evolutionary Genetics* 397–408 (2011).

70. Sive, H. L., Grainger, R. M. & Harland, R. M. *Early development of Xenopus laevis: a laboratory manual*. (2000).

71. Lesurf, R. *et al.* ORegAnno 3.0: A community-driven resource for curated regulatory annotation. *Nucleic Acids Research* **44**, 126–132 (2016).

72. Sullivan, C. H., Majumdar, H. D., Neilson, K. M. & Moody, S. A. Six1 and Irx1 have reciprocal interactions during cranial placode and otic vesicle formation. *Developmental Biology* **446**, 68–79 (2019).

73. Hanotel, J. *et al.* The Prdm13 histone methyltransferase encoding gene is a Ptf1a-Rbpj downstream target that suppresses glutamatergic and promotes GABAergic neuronal fate in the dorsal neural tube. *Developmental Biology* **386**, 340–357 (2014).

74. Bessodes, N., Parain, K., Bronchain, O., Bellefroid, E. J. & Perron, M. Prdm13 forms a feedback loop with Ptf1a and is required for glycinergic amacrine cell genesis in the Xenopus Retina. *Neural Development* **12**, (2017).

75. Ghiasvand, N. M. *et al.* Deletion of a remote enhancer near ATOH7 disrupts retinal neurogenesis, causing NCRNA disease. *Nature Neuroscience* **14**, 578–588 (2011).

76. Bhatia, S. *et al.* Disruption of autoregulatory feedback by a mutation in a remote, ultraconserved PAX6 enhancer causes aniridia. *American Journal of Human Genetics* **93**, 1126–1134 (2013).

77. Radziwon, A. *et al.* Single-base substitutions in the CHM promoter as a cause of choroideremia. *Human Mutation* **38**, 704–715 (2017).

78. Mona, B. *et al.* Repression by PRDM13 is critical for generating precision in neuronal identity. *eLife* **6**, (2017).

79. Watanabe, S. *et al.* Prdm13 regulates subtype specification of retinal amacrine interneurons and modulates visual sensitivity. *Journal of Neuroscience* **35**, 8004–8020 (2015).

80. Green, D. J. *et al.* North Carolina macular dystrophy: Phenotypic variability and computational analysis of disease-associated noncoding variants. *Investigative Ophthalmology and Visual Science* **62**, (2021).

81. Kwong, J. M. K. *et al.* Co-expression of heat shock transcription factors 1 and 2 in rat retinal ganglion cells. *Neuroscience Letters* **405**, 191–195 (2006).

82. Hafezi, F., Marti, A., Grimm, C., Wenzel, A. & Remé, C. E. Differential DNA binding activities of the transcription factors AP-1 and Oct-1 during light-induced apoptosis of photoreceptors. *Vision Research* **39**, 2511–2518 (1999).

83. Provis, J. M., van Driel, D., Billson, F. A. & Russell, P. Development of the Human Retina: Patterns of Cell Distribution and Redistribution in the Ganglion Cell Layer. *The Journal of Comparative Neurology* **233**, 429–451 (1985).

84. Franke, M. *et al.* Formation of new chromatin domains determines pathogenicity of genomic duplications. *Nature* **538**, 265–269 (2016).

85. Tena, J. J. *et al.* An evolutionarily conserved three-dimensional structure in the vertebrate Irx clusters facilitates enhancer sharing and coregulation. *Nature Communications* **2**, 310 (2011).

86. Bosse, A. *et al.* Identification of the vertebrate Iroquois homeobox gene family with overlapping expression during early development of the nervous system. *Mechanisms of Development* **69**, 169–181 (1997).

87. Cohen, D. R., Wa Cheng, C., Han Cheng, S. & Hui, C. Expression of two novel mouse Iroquois homeobox genes during neurogenesis. *Mechanisms of Development* **91**, 317–321 (2000).

88. Cheng, C. W., Yan, C. H. M., Hui, C. Chung, Strähle, U. & Cheng, S. H. The homeobox gene irx1a is required for the propagation of the neurogenic waves in the zebrafish retina. *Mechanisms of Development* **123**, 252–263 (2006).

89. Voigt, A. P. *et al.* Human photoreceptor cells from different macular subregions have distinct transcriptional profiles. *Human Molecular Genetics* **30**, 1543–1558 (2021).

90. Hoshino, A. *et al.* Molecular Anatomy of the Developing Human Retina. *Developmental Cell* **43**, 763–779 (2017).

91. Nekolova, J., Stepanov, A., Kousal, B., Stredova, M. & Jiraskova, N. Modern diagnostic and therapeutic approaches in familial maculopathy with reference to North Carolina macular dystrophy. *Biomedical Papers* (2021) doi:10.5507/bp.2021.037.

Figures & tables

Figure 1 - Integration of UMI-4C interaction frequency profiles and domainograms (bottom) for the *PRDM13* promoter (left) and *IRX1* promoter (right) viewpoints, with Hi-C data from control human retinal organoids (top).[40] Topologically associated domains (TADs) are indicated by blue triangles. Chromosome coordinates are in hg38 annotation.

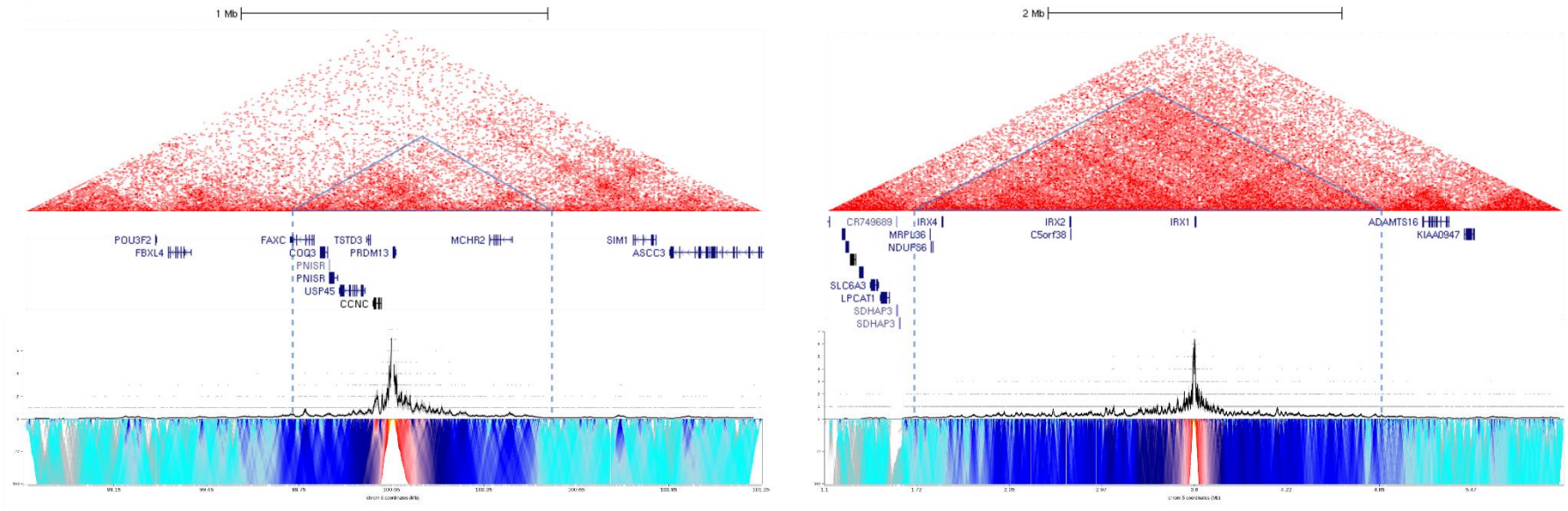

Table 1 - Overview of cCREs in the *PRDM13* and *IRX1* loci, obtained after integration of the UMI-4C profiles in the retina-specific multi-omics database. The regions were selected based on the presence of both a UMI-4C peak and an element of interest and are visualized in Suppl. Figure 3. ATAC: assay for transposase accessible chromatin, cCRE: candidate CRE, ChIP: chromatin immunoprecipitation, DHS: DNase I hypersensitive site, MHS: mutational hotspot, UCNE: ultraconserved non-coding element.

cCRE	Coordinates (hg38)	Element of interest
PRDM13 locus		
cCRE1	chr6:99,588,208-99,589,239	DHS, ChIP peak
cCRE2	chr6:99,590,566-99,591,414	DHS
cCRE3	chr6:99,595,852-99,596,746	ATAC HSR, ChIP peak
cCRE4	chr6:99,598,651-99,599,224	MHS2, DHS
cCRE5	chr6:99,617,828-99,619,867	DHS
cCRE6	chr6:99,645,605-99,647,017	DHS
cCRE7	chr6:99,749,318-99,752,123	UCNE (PRDM13_Brooklyn), DHS
IRX1 locus		
cCRE8	chr5:3,224,667-3,227,420	UCNE (IRXA_Scout)
cCRE9	chr5:3,426,706-3,428,595	UCNE (IRXA_Santagio_1, IRXA_Santagio_2)
cCRE10	chr5:3,488,008-3,490,747	UCNE (IRXA_Ryan)
cCRE11	chr5:3,529,207-3,531,844	UCNE (IRXA_Eden), DHS
cCRE12	chr5:3,620,470-3,622,600	DHS
cCRE13	chr5:3,628,385-3,630,819	DHS
cCRE14	chr5:3,649,694-3,651,723	DHS
cCRE15	chr5:3,729,667-3,732,532	ATAC HSR
cCRE16	chr5:3,786,388-3,788,778	DHS

Figure 2 - The UMI-4C data (green) from the *PRDM13* promoter viewpoint (right gray bar) illustrate an interaction with cCRE1 (left gray bar), a non-coding region upstream of the promoter (left arrow). Since underlying epigenomic tracks show an overlap of this region with DNase-seq (turquoise) and ATAC-seq (green) peaks, as well as with ChIP-seq profiles of specific histone marks indicative of enhancer activity (H3K27ac, H3K4me2) (yellow) and ChIP-seq profiles of retinal TFs (CRX, NRL, OTX2) (orange), this region is a strong cCRE. The reverse UMI-4C experiment using this cCRE as a viewpoint, results in a peak around the *PRDM13* promoter region (right arrow), confirming this interaction. cCRE: candidate CRE.

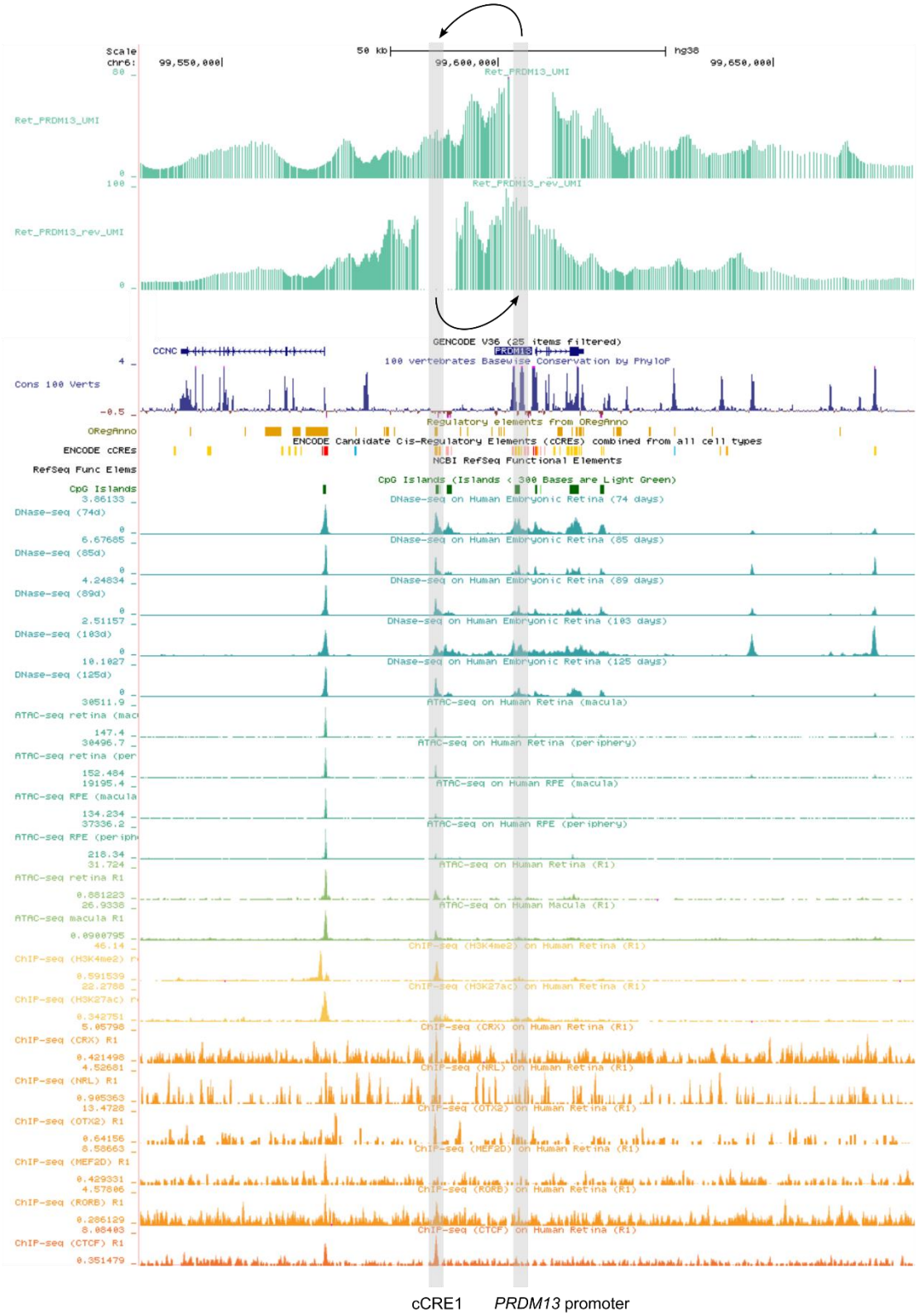

Figure 3 - Single-cell transcriptomic analysis of developing human neural retina. In particular, data from six embryonic (53, 59, 74, 78, 113, and 132 days) and three adult (25, 50, and 54 years old) human retinal samples are included. (**A**) UMAP plot of 60,014 human neural retinal cells from all samples, colored based on the ten transcriptionally distinct clusters represented in the key. (**B-C**) The different retinal samples were grouped into four time points: e50 = d53 and d59, e70 = d74 and d78, e100 = d113 and d132, adult = 3 samples. Violin plots respectively illustrate *PRDM13* and *IRX1* expression in the different retinal cell types for each of these time points.

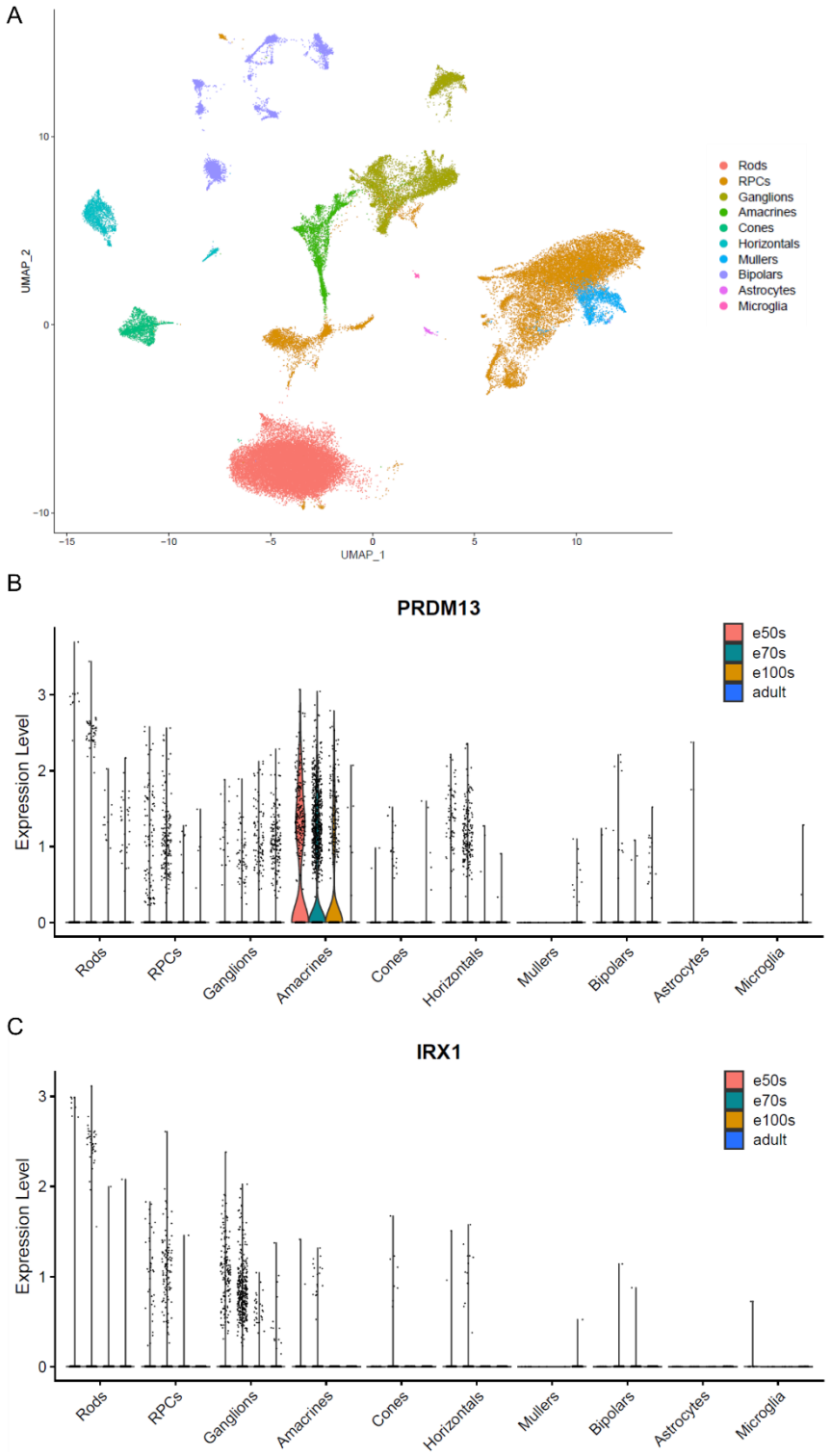

Figure 4 - Overview of previously reported and novel (likely) pathogenic variants (V) in the *PRDM13* locus (left) and *IRX1* locus (right). Known and novel SNVs are indicated by red and green bars, respectively. The two mutational hotspots (MHS1, MHS2), the second one of which overlaps with cCRE4, and the shared duplicated region (SDR) spanning a UCNE are highlighted by grey bars. The pathogenic tandem duplications are shown as blue bars, while benign duplications spanning the *IRX1* coding region, derived from DGV, are shown as pink bars. The DNase-seq track was generated in human embryonic retinal tissue at day 103 of development. Chromosome coordinates are in hg38 annotation. cCRE: candidate CRE, MHS: mutational hotspot, SDR: shared duplicated region, UCNEs: ultraconserved non-coding elements.

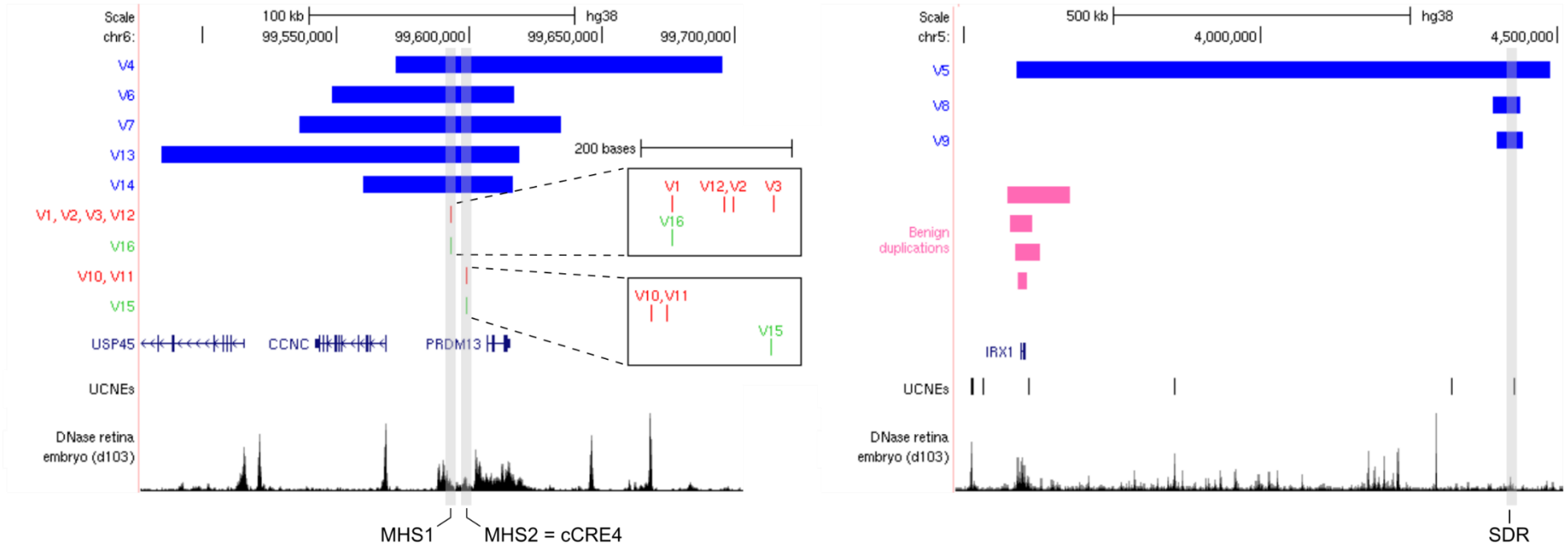

Table 2 - Overview of the previously reported and novel NCMD-associated SNVs (V) in the two mutational hotspots (MHS) upstream of *PRDM13*. For each variant, the coordinates (hg38), nucleotide change, gnomAD frequency, and TRANSFAC output are given, as well as the prediction scores and the PHRED-scaled scores ($-10\log_{10}\frac{rank}{total}$) of seven *in silico* tools. The regBase_REG and regBase_PAT scores range from 0 to 1, with higher values indicating that a variant has a higher regulatory or pathogenic potential, respectively. GenoCanyon scores range from 0 to 1. A cutoff of 0.5 was used to define functionality. The ncER score ranges from 0 to 100, with higher scores suggesting that a region is more vital in terms of regulation. DVAR scores, ranging from 0 to 1, can be interpreted as the probability of a variant being functional. The FIRE score also ranges from 0 to 1, with higher scores providing stronger evidence that a variant regulates nearby gene expression levels. PAFA scores range from -1 to 1, reflecting the association of a variant with complex diseases or trait-associated SNPs. The CDTS score represents the absolute difference of the observed variation from the expected variation, with lower scores suggesting more intolerance to variation. The normalized, PHRED-scaled scores are color-coded for easy comparison (green = high, red = low).

Name	Coordinates	gnomAD	TRANSFAC TFBS	regBase REG	regBase REG PHRED	regBase PAT	regBase PAT PHRED	Geno Canyon	Geno Canyon PHRED	ncER	ncER PHRED	DVAR	DVAR PHRED	FIRE	FIRE PHRED	PAFA	PAFA PHRED	CDTS	CDTS PHRED
MHS1																			
V1	chr6:99593030G>T	-	-	0.92	15.58	0.86	19.78	1.00	16.61	81.34	7.33	0.89	9.38	0.59	7.48	0.94	11.61	-2.30	5.53
V16	chr6:99593030G>C	-	-	0.90	14.07	0.79	18.37	1.00	16.61	81.34	7.33	0.89	9.38	0.59	7.36	0.94	11.61	-2.30	5.53
V12	chr6:99593098A>C	-	-	0.85	10.94	0.16	8.34	1.00	15.14	73.37	5.79	0.89	9.39	0.57	7.16	-0.44	0.88	1.06	2.60
V2	chr6:99593111G>C	6.6E-06	-	0.92	15.42	0.85	19.53	1.00	16.32	79.83	7.00	0.90	9.70	0.58	7.31	-0.34	1.09	0.99	2.65
V3	chr6:99593164C>T	-	-	0.90	14.09	0.71	16.98	1.00	14.02	69.37	5.18	0.89	9.36	0.60	7.60	-0.59	0.65	-0.96	4.11
MHS2																			
V10	chr6:99598907A>C	-	POU2F1 loss	0.71	5.97	0.08	5.76	0.00	2.31	15.60	0.78	0.75	6.03	0.64	8.20	0.30	5.06	-1.74	4.89
V11	chr6:99598928T>C	-	-	0.80	8.56	0.02	1.34	0.00	2.51	10.99	0.55	0.76	6.14	0.65	8.45	0.23	4.60	-1.67	4.82
V15	chr6:99599064A>G	-	HSF1 gain	0.75	7.05	0.04	3.42	0.00	2.28	31.48	1.69	0.72	5.45	0.64	8.33	0.39	5.69	2.73	1.81

Figure 5 - Overview of the *in vitro* mutant versus WT luciferase assays in ARPE-19 cells. (**A**) In the first mutational hotspot (MHS1), the four known variants and one novel variant (V) demonstrate a significant increase of luciferase reporter activity (P<0.001), relative to the WT vector (MHS1). (**B**) In contrast, the two known and one novel variant located in the second mutational hotspot (MHS2), cause a significant decrease of luciferase reporter activity (P<0.001), relative to the WT vector (MHS2). (**C**) For three non-coding regions of interest, located in the shared duplicated region of either the *PRDM13* (MHS1, cCRE1) or *IRX1* locus (SDR), the level of luciferase reporter was reduced by half (P<0.001) when the region was present as tandem duplication, relative to their respective WT counterpart, containing the same region of interest as a single insert. cCRE: candidate CRE, MHS: mutational hotspot, SDR: shared duplicated region.

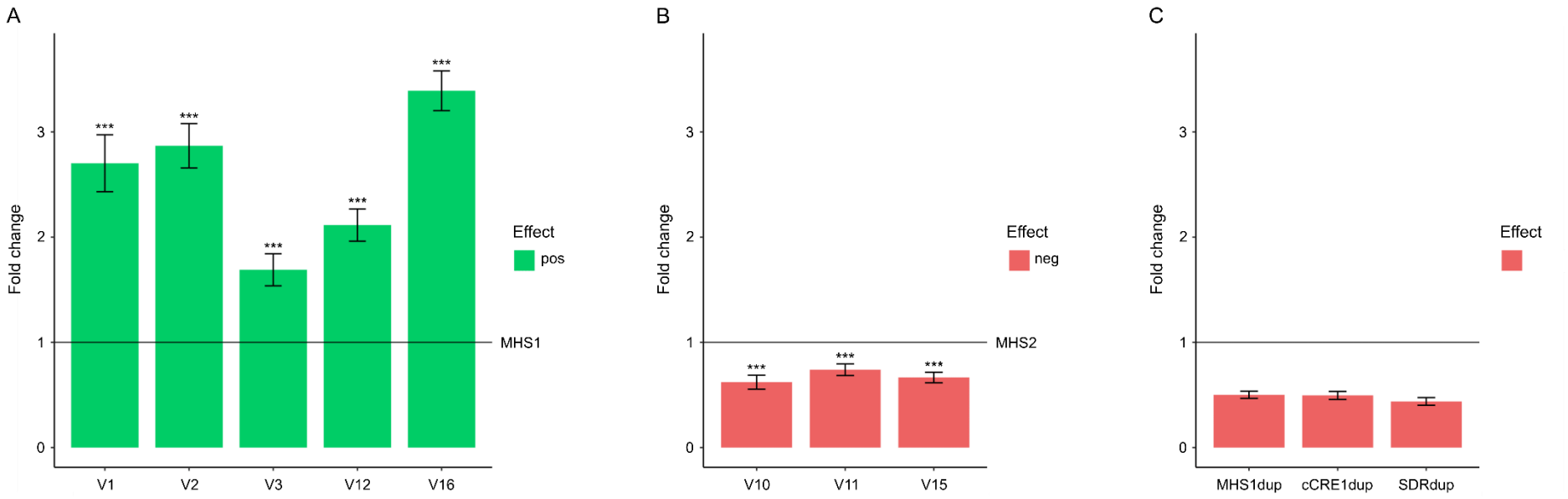

Figure 6 - Representative images of EGFP reporter expression in living, transgenic *Xenopus* tadpoles, driven by SED vector reporter constructs containing non-coding regions of interest. The respective *Xenopus* species injected and the Nieuwkoop and Faber (NF) stage shown in the pictures are indicated on top of the images, while the injected construct and the stage of injection are indicated on the left side of the images. For each stage, the number of tadpoles displaying the depicted EGFP reporter expression pattern over the total number of analyzed transgenic tadpoles is given. (**A,B**) Dorsal view of transgenic *Xenopus tropicalis* embryos upon unilateral injection of the reporter construct containing cCRE14. EGFP reporter expression was visible at the neural plate and tube (NP) on the injected side, indicated by the arrow, while no expression was observed on the non-injected side. (**C,D**) Ventral view of transgenic tadpoles, displaying EGFP reporter expression in the craniofacial cartilage, a derivative of the neural crest (NC), and the eye (E) on the injected side. (**E,F**) At the same stages, DsRed (positive control) expression was apparent in the myotomes (M) of the tadpoles. (**G,H**) Detailed view of the eye at NF stage 55 indicates EGFP reporter expression was maintained on the injected (left) side, while no expression was observed in the non-injected (right) side. (**I,J**) Lateral and dorsal view of transgenic albino *Xenopus laevis* tadpoles upon unilateral injection of the reporter construct containing cCRE14 in the two-cell stage demonstrated EGFP reporter expression in the eye and brain (B). (**K,L**) Lateral and dorsal view of transgenic tadpoles injected with the same construct, but in two of the dorsal blastomeres at the four-cell stage, also displayed EGFP reporter expression in the eye and brain. (**M,N**) Lateral and dorsal view of transgenic tadpoles introduced with SDR reporter construct demonstrated low EGFP reporter expression in the eye and brain. (**O-Q**) DsRed (positive control) was expressed in the myotomes of the corresponding tadpoles. (**R**) Lateral view of transgenic albino *Xenopus laevis* tadpoles upon injection of the reporter construct containing MHS1 showed no EGFP reporter expression in the eye or brain. (**S,T**) Lateral and dorsal view of transgenic tadpoles injected with MHS2 (cCRE4) (**U,V**) or cCRE1 demonstrated EGFP reporter expression in the eye and brain.

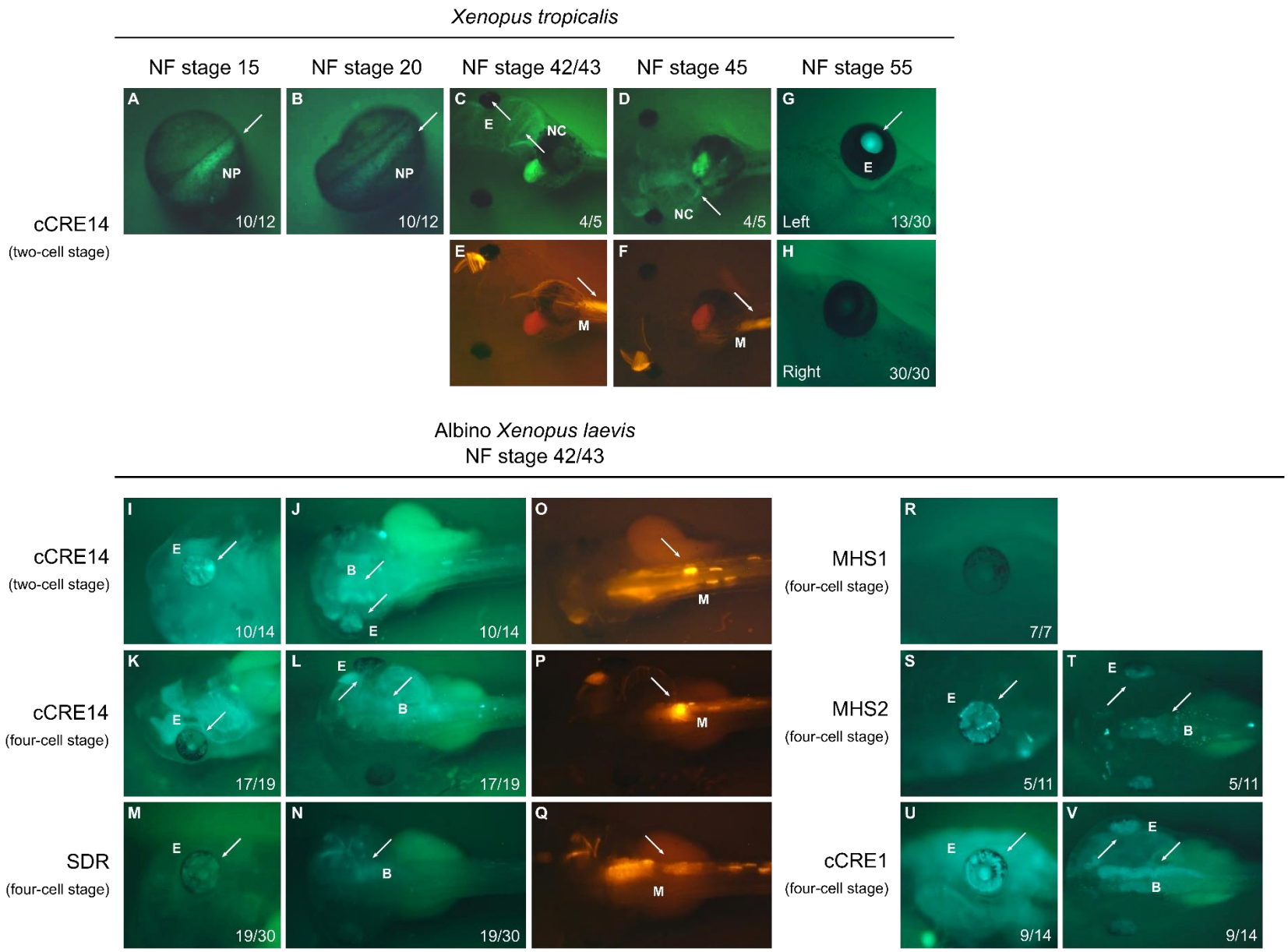
Xenopus tropicalis
NF stage 15
NF stage 20
NF stage 42/43
NF stage 45
NF stage 55
cCRE14
(two-cell stage)
A
NP
10/12
B
NP
10/12
C
E
NC
4/5
D
NC
4/5
G
E
Left
13/30
E
M
F
M
H
Right
30/30
Albino Xenopus laevis
NF stage 42/43
cCRE14
(two-cell stage)
I
E
10/14
J
B
E
10/14
O
M
MHS1
(four-cell stage)
R
7/7
cCRE14
(four-cell stage)
K
E
17/19
L
E
B
17/19
P
M
MHS2
(four-cell stage)
S
E
5/11
T
E
B
5/11
SDR
(four-cell stage)
M
E
19/30
N
B
19/30
Q
M
cCRE1
(four-cell stage)
U
E
9/14
V
E
B
9/14

Supplementary data

Suppl. Table 1 - Overview of the qPCR primers used for assessing the purity of the retinal tissue on which UMI-4C was performed.

Gene name	F primer	R primer
Retina		
CRX	5'-ATCTGATGCACCAGGCTGT-3'	5'-GACGTCTGGGTACTGGGTCT-3'
RHO	5'-ACATGTTCGTGGTCCACTTC-3'	5'-CAGCGGCCTCCTTGAC-3'
OPN1LW	5'-TCTCTGGCTACTTCGTGCTG-3'	5'-AGGAAATGATGGCCAGAGAC-3'
Interphotoreceptor matrix		
RBP3	5'-TGGAGCACATCTGGAAGAAG-3'	5'-AGATGGGAATGGAGGATGTG-3'
Retinal pigment epithelium		
RPE65	5'-GGCTCCAGCCAGATAGTCTC-3'	5'-AGAAAGGCTCCCCAACCT-3'
Reference genes		
GUSB	5'-AGAGTGGTGCTGAGGATTGG-3'	5'-CCCTCATGCTCTAGCGTGTC-3'
SDHA	5'-TGGGAACAAGAGGGCATCTG-3'	5'-CCACCACTGCATCAAATTCATG-3'
GAPDH	5'-GTCGGAGTCAACGGATTT-3'	5'-GGCAACAATATCCACTTTACC-3'

Suppl. Table 2 - Overview of the US and DS primers used for generating the UMI-4C libraries. cCRE: candidate CRE, SDR: shared duplicated region.

Viewpoint	US primer	DS primer
PRDM13 promoter	5'-caaaccagttttgggaaata-3'	5'-ctacttggctgattcctttg-3'
IRX1 promoter	5'-gggtttccctgtaacttttc-3'	5'-tgcctttcaggtctcttact-3'
cCRE1 (*PRDM13*)	5'-aaggctgtgtgtacgttcc-3'	5'-aggtacaggaggaatttcaa-3'
SDR (*IRX1*)	5'-ataccacagaaccaggacac-3'	5'-tgctttctcactctgtgcta-3'

Suppl. Table 3 - Overview of the PCR primers used for screening the known NCMD-associated SNVs and tandem duplications, and the qPCR primers used for performing the copy number analysis in the two NCMD-associated disease loci.

Variant	F primer	R primer
Known SNVs		
V1-V3 & V12	5'-GAGAAGACTAGATCAGGCTTCTTC-3'	CTCTCATTCTCTGATTTTTAC-3'
V10-V11	5'-TCCTATGTCTTGAGTGCTCTGC-3'	AAATGCCCAACACATAACAGG-3'
Tandem duplications		
V4	5'-ACACAATATGCTCCTGAATGAA-3'	GGAAGAAGAGTGCAGAATTAGG-3'
V5	5'-GTTTTCACGAAAGTGCAAAGG-3'	GGGGTGGAAGAGAAGAGAGG-3'
V6	5'-CATGGGAAACATTTTATCAGC-3'	TGTTGATGTTTCTTGGCCT-3'
V7	5'-CCAGTGGTTGGATACTGGTG-3'	CTCATAAGAGTTTTGTTGGCATAA-3'
V8	5'-TTTGCTTGATCAATTCTGCTG-3'	TTCTCAGTTGGAAGAGCACAAA-3'
V9	5'-AAATGGCTTCCAGTCACCAG-3'	GGCAATGCTTGCTTATGAGG-3'
Copy number analysis		
PRDM13 exon 1	5'-CAGCCACCAGCGTGAGT-3'	GACAGGTACTTGCCCAGCTT-3'
PRDM13 exon 2	5'-GAACGACCACTGCTTGTGTT-3'	CTGTTCCTGGGAGTTTCTGG-3'
PRDM13 exon 3	5'-CTACCGAGCATTGCGAGAC-3'	GGGATGTCGAACCACTGAG-3'
PRDM13 exon 4	5'-CTCGGTCTCTCCCCAAAAC-3'	GCAGGCCTGAACTGGTG-3'
IRX1 exon 1	5'-CTCTTCTCGCAGATGGTGAG-3'	CAGGTCCACCCGTAGTCTCT-3'
IRX1 exon 2	5'-ACGAGGATGACGAGGACAA-3'	AGTCCTGGGGCTTGAGAAC-3'
IRX1 exon 3	5'-GTCCCCAGGCCAGATTC-3'	TCCCATAGCAAAAGCAAACA-3'
IRX1 exon 4	5'-GTGCCCCTGTCTTCTTGTCT-3'	GACGGGAGGGCTGCTA-3'
IRX1 V8-V9 region	5'-GGCTTACAAGTATGACTGTTCTCC-3'	TTTCATGACACTTTGCAAACAC-3'

Suppl. Table 4 - Overview of the genomic regions that were cloned into pGL4.23 luciferase reporter vectors, together with their respective PCR primers. cCRE: candidate CRE, MHS: mutational hotspot, SDR: shared duplicated region

Region	Coordinates (hg38)	F primer	R primer	Size (bp)
Non-coding regions of interest				
MHS1	chr6:99,592,707-99,593,515	5'-ACAGGTACCTCATTCAGAGGAGGGGTAGC-3'	5'-ACAGCTAGCCCCAATGATGCTGGATAAAA-3'	809
MHS2 = cCRE4	chr6:99,598,569-99,599,474	5'-ACAGGTACCCCAGAAGTCCTGCTCCATTT-3'	5'-ACAGCTAGCAAACCGTCTTCCAAAGCAGC-3'	906
cCRE1	chr6:99,588,187-99,589,433	5'-ACAGGTACCGGAAGATCCCTCCAATCACA-3'	5'-ACAGCTAGCGCTCTCGCAGCTGTTTAGGT-3'	1247
cCRE5	chr6:99,618,274-99,619,518	5'-ACAGGTACCTGCAGAACACTCTCCTCTTGG-3'	5'-ACAGCTAGCCTTGGAGGGTTTGCAAGCTA-3'	1245
cCRE7	chr6:99,749,229-99,750,379	5'-ACAGGTACCCTGATGAGAAGGTGCTTAGCC-3'	5'-ACAGCTAGCAACACACTCATTCACTTGCATTG-3'	1151
cCRE8	chr5:3,226,007-3,227252	5'-ACAGGTACCTAGAGCCCGATGGATTATGG-3'	5'-ACAGCTAGCCAAATGGACACACGGTTCTG-3'	1246
cCRE9	chr5:3,427,612-3,428,807	5'-ACAGGTACCTTATTCATGATGCGGAAGCA-3'	5'-ACAGCTAGCCAACGCAATGAGGCAGTTTA-3'	1196
cCRE10	chr5:3,489,285-3,490,384	5'-ACAGGTACCCGACTGTCCAGCGATCAATA-3'	5'-ACAGCTAGCTTTGCCTTTTCCGAAATCAC-3'	1100
cCRE11	chr5:3,530,408-3,532,022	5'-ACAGCTAGCTGCATATGCTGATGCCTTCT-3'	5'-ACACTCGAGCCCTTTCTAGGGACCCTCAC-3'	1615
cCRE12	chr5:3,620,757-3,622,296	5'-ACAGGTACCGGCCAGCTTGACAACAGTTT-3'	5'-ACAGCTAGCTCACCCTTGCTGCCTAACTC-3'	1540
cCRE13	chr5:3,629,215-3,630,688	5'-ACAGGTACCGGGAAGAGCTACAAGCACCT-3'	5'-ACAGCTAGCGACTGACCACCCAACTCCTC-3'	1474
cCRE14	chr5:3,650,013-3,651,313	5'-ACAGGTACCTTTATACGGGGCTTCCCTTT-3'	5'-ACAGCTAGCTGGAGGACCTATGGGAACTG-3'	1301
cCRE15	chr5:3,730,531-3,731,978	5'-ACAGGTACCCTCAGGCTTTCATGCTTTGA-3'	5'-ACAGCTAGCGGCTGGACATGGAAAAGATG-3'	1448
SDR	chr5:4,424,475-4,425,443	5'-ACAGGTACCGGCTGTCAACCTCCAACATT-3'	5'-ACAGCTAGCGCATGCAATGCTTTTCAAGAAC-3'	969
Reference control regions with no indication of regulatory activity				
Ctrl1	chr18:941,974-942,906	5'-ACAGGTACCTGCCCACAACCCTACAATTA-3'	5'-ACAGCTAGCGCCCAGTAGAAGCTATTCCTTTC-3'	933
Ctrl2	chr18:941,609-943,005	5'-ACAGGTACCTCTTAGGGCATCAGGGTCAG-3'	5'-ACAGCTAGCGAAGGCATATTTCTAGCCCACT-3'	1397

Suppl. Table 5 - Overview of the mutagenesis primers used for introducing the different SNVs into pGL4.23 luciferase reporter vectors containing the respective region of interest. MHS: mutational hotspot.

Variant	Region	Coordinates (hg38)	F primer	R primer
Known SNVs				
V1	MHS1	chr6:99,593,030G>T	5'-CACATTTACTTATGTCCCACTG-3'	5'-ACACAAGCAGAAGTTTCAG-3'
V2	MHS1	chr6:99,593,111G>C	5'-ATGAATACCACGAGGTTCAATTCAC-3'	5'-GCTCTTGCATAATCTCCTTTC-3'
V3	MHS1	chr6:99,593,164C>T	5'-AGGAAATTAATCCCAGAAGAG-3'	5'-GTAGCAAACTGTTACATAATC-3'
V10	MHS2	chr6:99,598,907A>C	5'-TAACTTAATCCTTTGCATAGAGAAGAAC-3'	5'-CCACGGGACATCATAGTAG-3'
V11	MHS2	chr6:99,598,928T>C	5'-GAAGAACAGACATGTGACATCAATTAAG-3'	5'-TCTATGCAAATGATTAAGTTAC-3'
V12	MHS1	chr6:99,593,098A>C	5'-ATTATGCAAGCGCATGAATACC-3'	5'-CTCCTTTCATAATGATCTTAAG-3'
Novel SNVs				
V15	MHS2	chr6:99,599,064A>G	5'-AACCTCTTTGGAATTTTCTCAC-3'	5'-AAGAAGCTTATTGGGGTC-3'
V16	MHS1	chr6:99,593,030G>C	5'-CACATTTACTCATGTCCCACTG-3'	5'-ACACAAGCAGAAGTTTCAG-3'

Suppl. Table 6 - Overview of the non-coding regions of interest that were cloned into SED reporter vectors, together with their respective PCR primers. cCRE: candidate CRE, MHS: mutational hotspot, SDR: shared duplicated region.

Region	Coordinates (hg38)	F primer	R primer	Size (bp)
MHS1	chr6:99,592,707-99,593,515	5'-ACAGGTACCTCATTCAGAGGAGGGGTAGC-3'	5'-ACAGCTAGCCCCAATGATGCTGGATAAAA-3'	809
MHS2 = cCRE4	chr6:99,598,569-99,599,474	5'-ACAGGTACCCCAGAAGTCCTGCTCCATTT-3'	5'-ACAGCTAGCAAACCGTCTTCCAAAGCAGC-3'	906
cCRE1	chr6:99,588,187-99,589,433	5'-ACAGGTACCGGAAGATCCCTCCAATCACA-3'	5'-ACAGCTAGCGCTCTCGCAGCTGTTTAGGT-3'	1247
cCRE14	chr5:3,650,013-3,651,313	5'-ACAGGTACCTTTATACGGGGCTTCCCTTT-3'	5'-ACAGCTAGCTGGAGGACCTATGGGAACTG-3'	1301
SDR	chr5:4,424,475-4,425,443	5'-ACAGGTACCGGCTGTCAACCTCCAACATT-3'	5'-ACAGCTAGCGCATGCAATGCTTTTCAAGAAC-3'	969

Suppl. Figure 1 - Schematic representation of the SED vector. The transgenesis internal control cassette is composed of the Cardiac Actin promoter (pink), driving strong expression in the somites, and the DsRed fluorescent protein (red), serving as a control for transgenesis efficiency *in vivo* in the F0 and the F1 embryos. The enhancer detection cassette contains a Gateway entry site (yellow), the *gata2* minimal promoter (light green), and the enhanced green fluorescent protein (EGFP) reporter gene (dark green). EGFP reporter expression can be observed during early development under a fluorescent microscope. Both cassettes are flanked by insulator sequences (purple) to protect them from position effects, and together they are flanked by I-*Sce*I meganuclease recognition sites (blue).

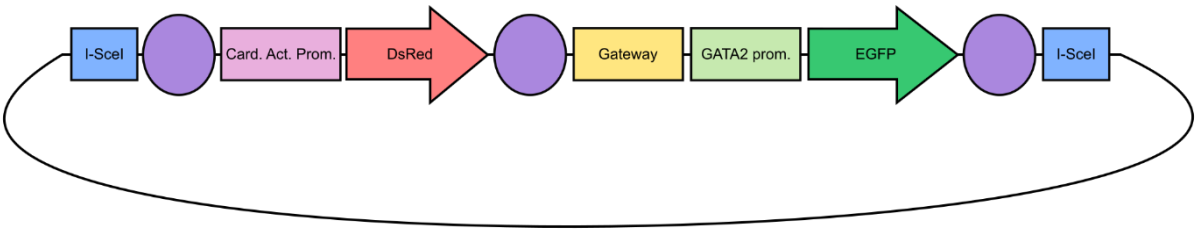

Suppl. Figure 2 - Output from the qPCR expression analysis of the two dissected retinal samples, compared against a control sample of RPE tissue. The retinal genes *CRX*, *RHO*, and *OPN1LW* are highly expressed in the retinal tissues, while expression of the RPE-specific *RPE65* gene is minimal relative to the RPE sample.

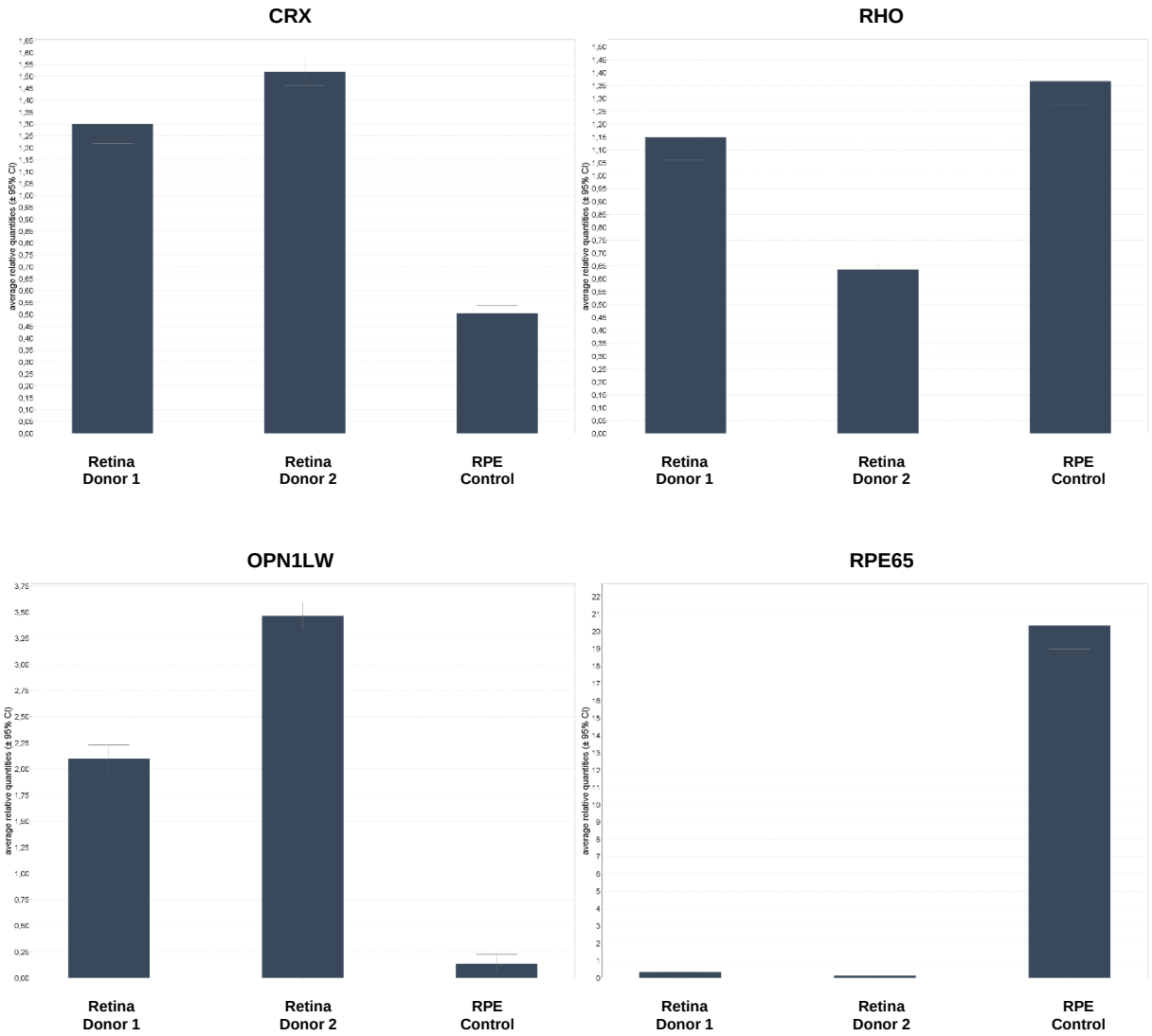

Suppl. Table 7 - Number of raw, mapped, and unique reads from UMI-4C sequencing of the different viewpoints.

Viewpoint	Sample	Raw	Mapped	UMIs
PRDM13 promoter	Donor 1	8,134,307	687,131	13,276
	Donor 2	7,330,735	290,656	20,842
IRX1 promoter	Donor 1	8,498,021	1,894,101	9,569
	Donor 2	4,890,848	1,555,296	15,694
cCRE1 (*PRDM13*)	Donor 1	4,445,807	967,751	7,150
	Donor 2	6,474,247	733,233	11,331
SDR (*IRX1*)	Donor 1	9,074,572	3,277,923	13,943
	Donor 2	7,542,129	2,704,943	18,199

Suppl. Figure 3 - Overview of cCREs in the (**A**) *PRDM13* and (**B**) *IRX1* locus, obtained after integration of the UMI-4C profiles in the retina-specific multi-omics database. The regions were selected based on the presence of both a UMI-4C peak and an element of interest. Known and novel pathogenic SNVs are respectively indicated as red and green bars, while previously reported tandem duplications are indicated as blue bars. cCRE: candidate CRE.

A

Scale
chr6:
99,600,000
50 kb
hg38
99,650,000
99,700,000
99,750,000
V4
V6
V7
V13
V14
V1, V2, V3, V12
V16
V10, V11
V15
Ret_PRDM13_UMI
GENCODE V38 (5 items filtered out)
PRDM13
100 vertebrates Basewise Conservation by PhyloP
Cons 100 Verts
Regulatory elements from ORegAnno
ORegAnno
ENCODE Candidate Cis-Regulatory Elements (cCREs) combined from all cell types
ENCODE cCREs
CpG Islands (Islands < 300 Bases are Light Green)
CpG Islands
Human/Chicken Ultraconserved Non-Coding Elements (UCNEs)
UCNEs
DNase-seq on Human Embryonic Retina (74 days)
DNase-seq (74d)
DNase-seq on Human Embryonic Retina (85 days)
DNase-seq (85d)
DNase-seq on Human Embryonic Retina (89 days)
DNase-seq (89d)
DNase-seq on Human Embryonic Retina (103 days)
DNase-seq (103d)
DNase-seq on Human Embryonic Retina (125 days)
DNase-seq (125d)
ATAC-seq on Human Retina (macula)
ATAC-seq retina (mac
ATAC-seq on Human Retina (periphery)
ATAC-seq retina (per
ATAC-seq on Human RPE (macula)
ATAC-seq RPE (macula
ATAC-seq on Human RPE (periphery)
ATAC-seq RPE (periph
ATAC-seq on Human Retina (R1)
ATAC-seq retina R1
ATAC-seq on Human Macula (R1)
ATAC-seq macula R1
ChIP-seq (H3K4me2) on Human Retina (R1)
ChIP-seq (H3K4me2) r
ChIP-seq (H3K27ac) on Human Retina (R1)
ChIP-seq (H3K27ac) r
ChIP-seq (H3K27ac) on Human Macula (R1)
ChIP-seq (H3K27ac) m
ChIP-seq (H3K27ac) on Human RPE (R1)
ChIP-seq (H3K27ac) R
ChIP-seq (CRX) on Human Retina (R1)
ChIP-seq (CRX) R1
ChIP-seq (NRL) on Human Retina (R1)
ChIP-seq (NRL) R1
ChIP-seq (OTX2) on Human Retina (R1)
ChIP-seq (OTX2) R1
ChIP-seq (MEF2D) on Human Retina (R1)
ChIP-seq (MEF2D) R1
ChIP-seq (RORB) on Human Retina (R1)
ChIP-seq (RORB) R1
ChIP-seq (CTCF) on Human Retina (R1)
ChIP-seq (CTCF) R1
ChIP-seq (CREB) on Human Retina (R1)
ChIP-seq (CREB) R1
cCRE
1
2
3
4
5
6
7

B

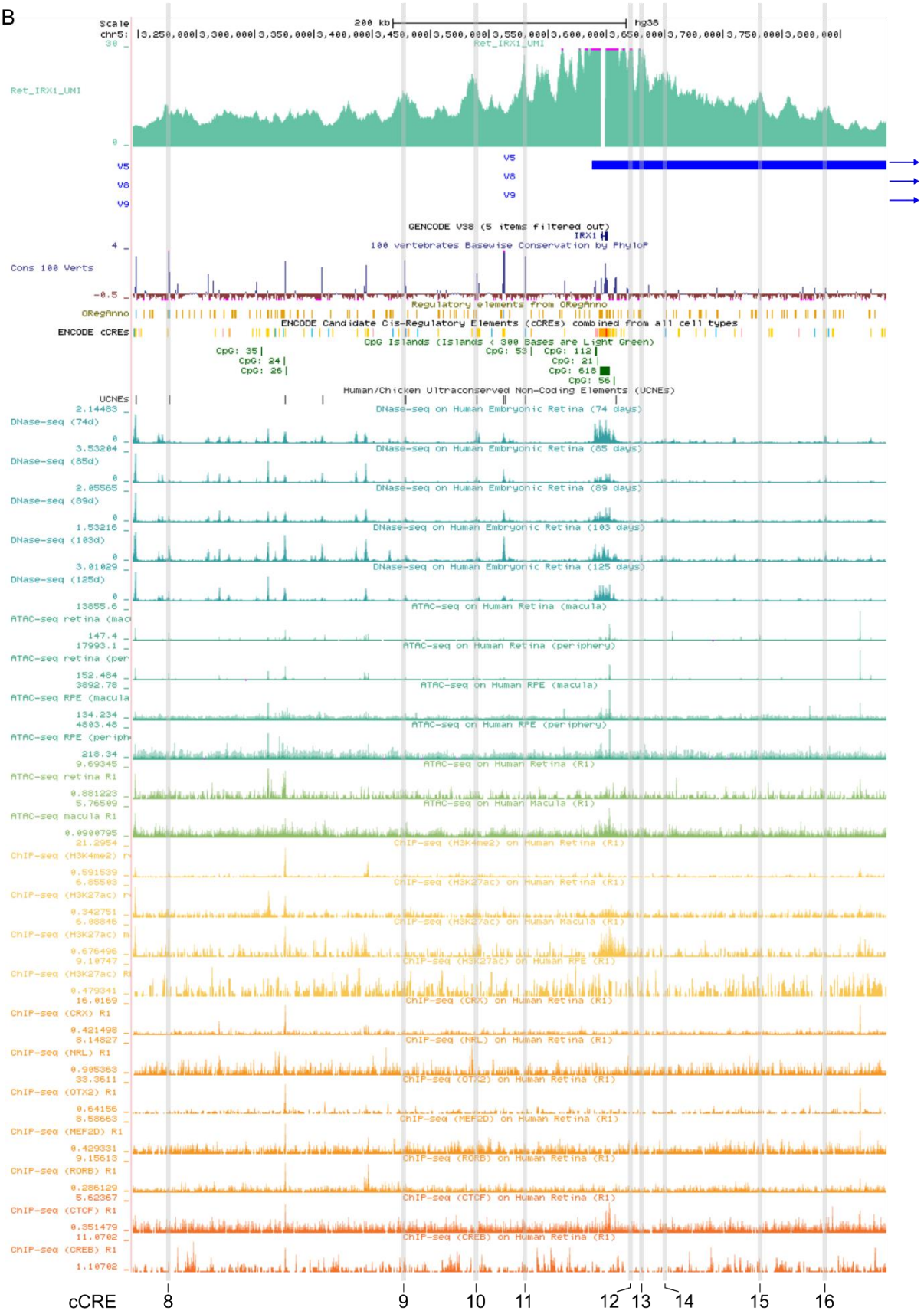
Scale
chr5: |3,250,000|3,300,000|3,350,000|3,400,000|3,450,000|3,500,000|3,550,000|3,600,000|3,650,000|3,700,000|3,750,000|3,800,000|
200 kb
hg38
Ret_IRX1_UMI
V5
V8
V9
GENCODE V38 (5 items filtered out)
IRX1
100 vertebrates Basewise Conservation by PhyloP
Cons 100 Verts
Regulatory elements from ORegAnno
ORegAnno
ENCODE Candidate Cis-Regulatory Elements (cCREs) combined from all cell types
ENCODE cCREs
CpG Islands (Islands < 300 Bases are Light Green)
Human/Chicken Ultraconserved Non-Coding Elements (UCNEs)
UCNEs
DNase-seq on Human Embryonic Retina (74 days)
DNase-seq (74d)
DNase-seq on Human Embryonic Retina (85 days)
DNase-seq (85d)
DNase-seq on Human Embryonic Retina (89 days)
DNase-seq (89d)
DNase-seq on Human Embryonic Retina (103 days)
DNase-seq (103d)
DNase-seq on Human Embryonic Retina (125 days)
DNase-seq (125d)
ATAC-seq on Human Retina (macula)
ATAC-seq on Human Retina (periphery)
ATAC-seq on Human RPE (macula)
ATAC-seq on Human RPE (periphery)
ATAC-seq on Human Retina (R1)
ATAC-seq retina R1
ATAC-seq on Human Macula (R1)
ATAC-seq macula R1
ChIP-seq (H3K4me2) on Human Retina (R1)
ChIP-seq (H3K27ac) on Human Retina (R1)
ChIP-seq (H3K27ac) on Human Macula (R1)
ChIP-seq (H3K27ac) on Human RPE (R1)
ChIP-seq (CRX) on Human Retina (R1)
ChIP-seq (CRX) R1
ChIP-seq (NRL) on Human Retina (R1)
ChIP-seq (NRL) R1
ChIP-seq (OTX2) on Human Retina (R1)
ChIP-seq (OTX2) R1
ChIP-seq (MEF2D) on Human Retina (R1)
ChIP-seq (MEF2D) R1
ChIP-seq (RORB) on Human Retina (R1)
ChIP-seq (RORB) R1
ChIP-seq (CTCF) on Human Retina (R1)
ChIP-seq (CTCF) R1
ChIP-seq (CREB) on Human Retina (R1)
ChIP-seq (CREB) R1
cCRE
8
9
10
11
12
13
14
15
16

Suppl. Figure 4 - The reverse UMI-4C experiment, using the shared duplicated region of the three previously reported NCMD-associated tandem duplications in the *IRX1* locus as a viewpoint. The UCNE located in this region is indicated by the horizontal arrow. The resulting UMI-4C profile suggests an interaction of this region with the *IRX1* promoter, as indicated by the diagonal arrow. However, in the UMI-4C experiment using the *IRX1* promoter as viewpoint, the interaction is less evident. The three tandem duplications are displayed as blue bars. SDR: shared duplicated region

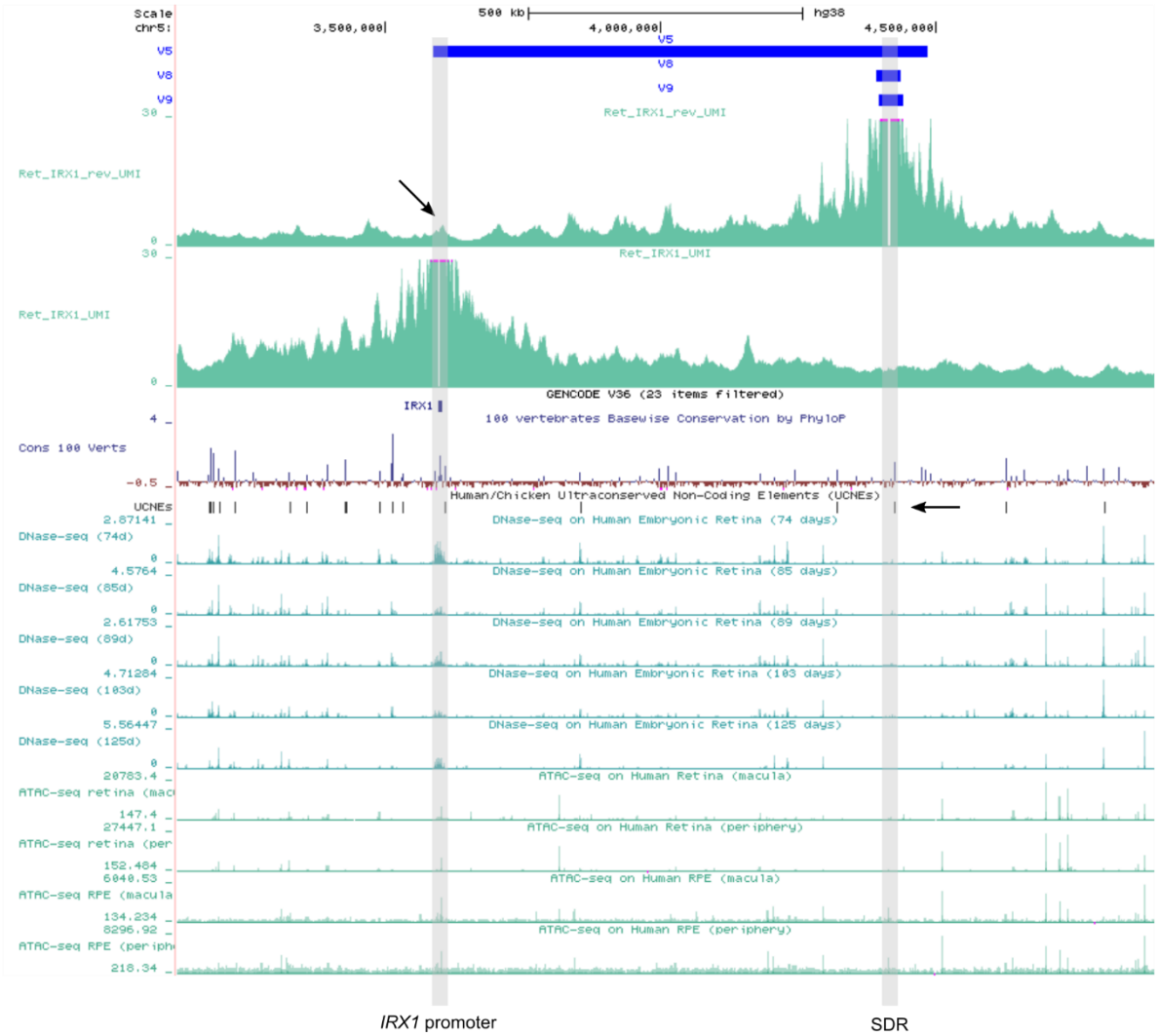

Suppl. Figure 5 - Single-cell transcriptomic analysis of developing human neural retina. UMAP plot showing expression of (**A**) *PRDM13* and (**B**) *IRX1* for four different time points (e50 = d53 and d59, e70 = d74 and d78, e100 = d113 and d132, adult = 3 samples) Plots are scaled to the maximum expression of *PRDM13* and *IRX1*, respectively. (**C**) Annotation of the ten transcriptionally distinct clusters.

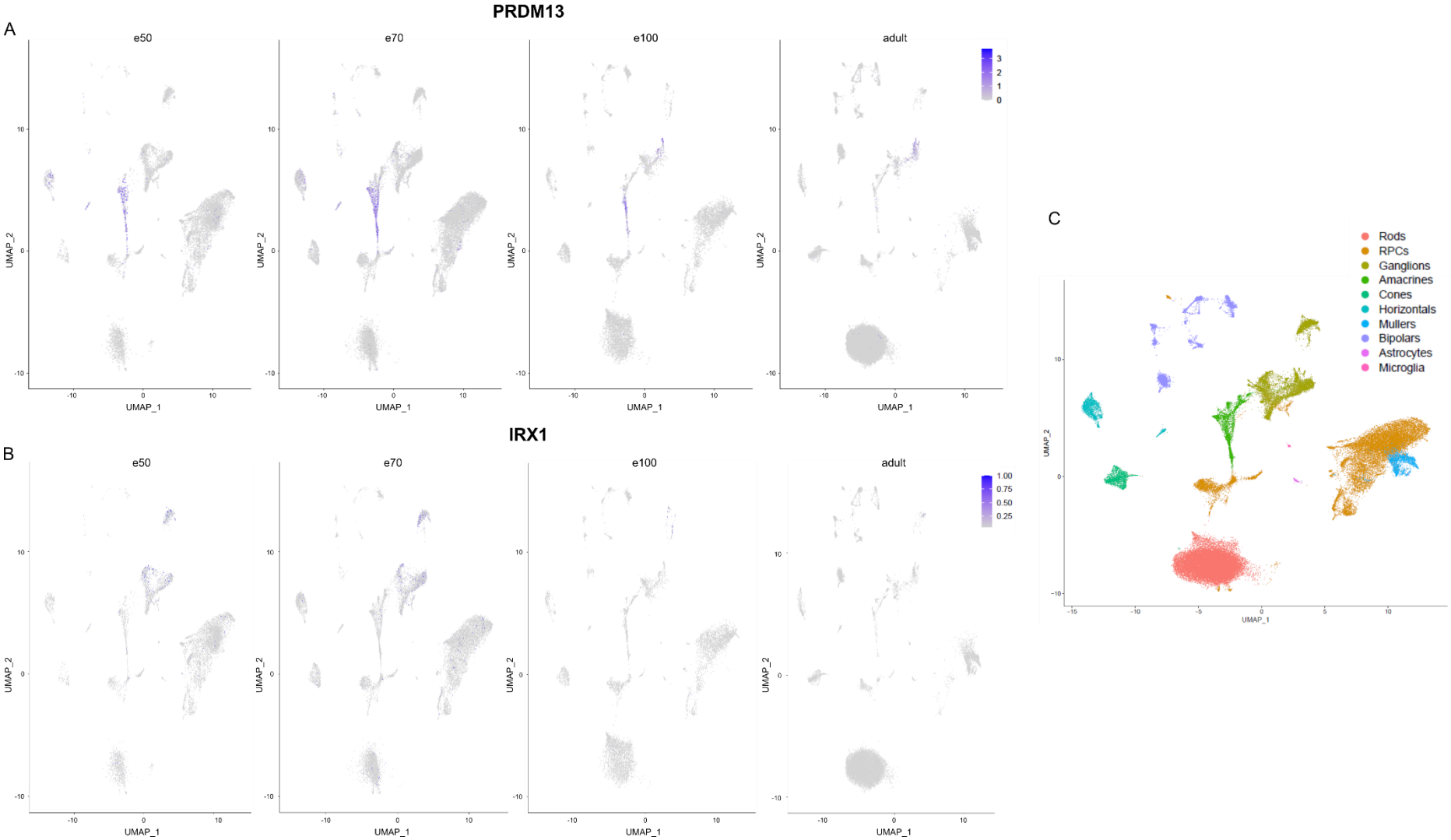

Suppl. Figure 6 - Overview of the genetic and clinical findings in **family F1**. (**A**) Pedigree of family F1. Individuals that were subjected to genetic testing are colored in red or green, respectively indicating whether the novel heterozygous **V15 variant** (chr6:99599064A>G) was present or not. (**B**) F1-III:1. Fundus BE (top): yellowish-white lesions in the macula, encircled by hypopigmented halos and surrounded by hyperpigmentation. OCT BE (bottom): focal RPE damage and focal neurosensory detachment. (**C**) F1-IV:1. Fundus BE (top): abnormality of macular pigmentation, drusen, focal RPE atrophy, and gross pigment deposits. OCT BE (bottom): focal RPE damage. RE: focal neurosensory detachment. LE: submacular scarring. (**D**) F1-IV:2. Fundus BE (top): mild RPE abnormalities with small macular drusen. OCT BE (bottom): mild RPE abnormalities with small macular drusen. (**E**) F1-II:3. Fundus BE (top): chorioretinal macular atrophy with fibrotic changes more pronounced in the LE. OCT BE (bottom): chorioretinal macular atrophy with fibrotic changes more pronounced in the LE, and vitreofoveal adhesion. This family was previously clinically described by Nekolova *et al.* (2021).[91] LE: left eye, RE: right eye, BE: both eyes.

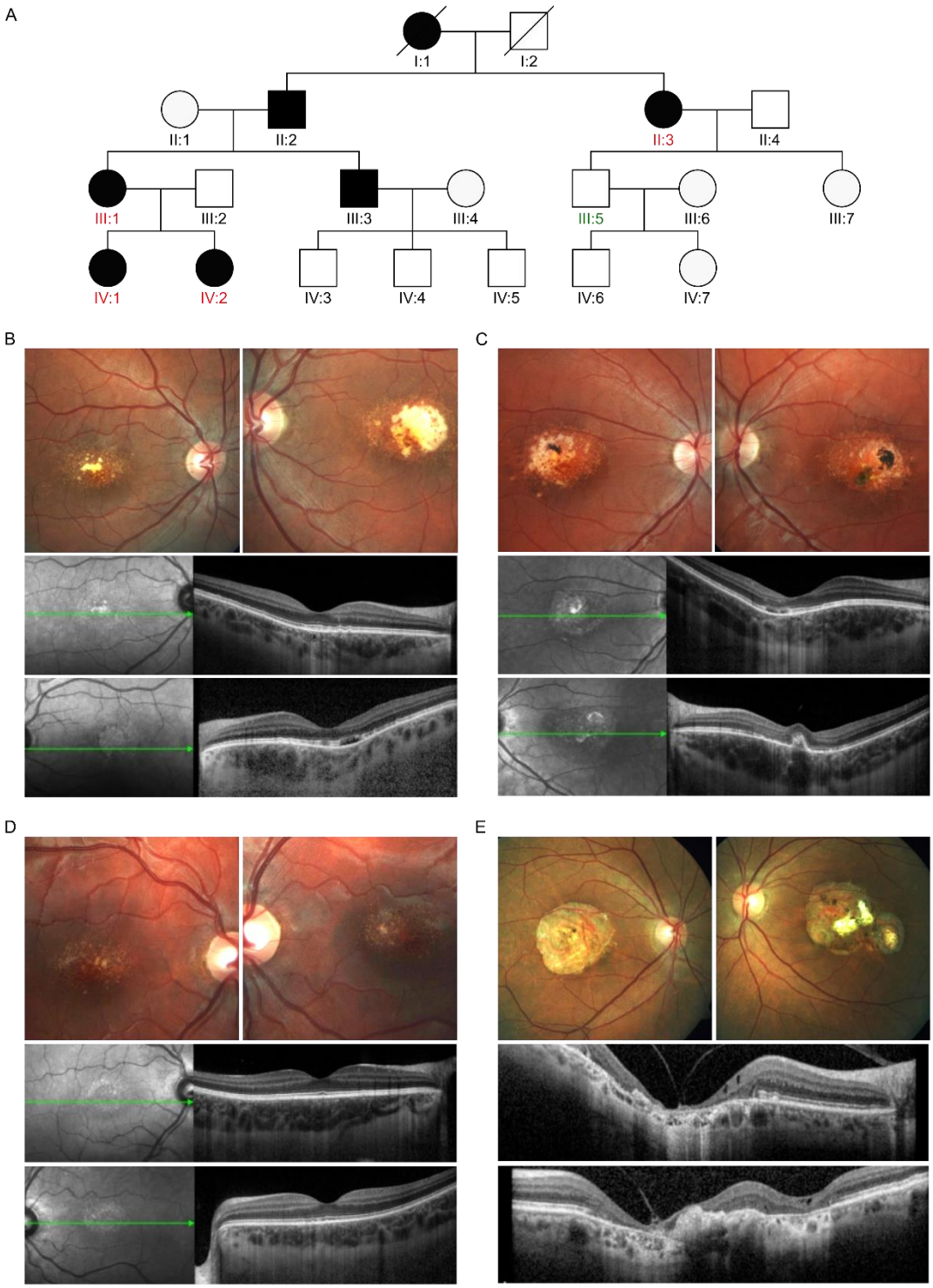

Suppl. Figure 7 - Overview of the genetic and clinical findings in **family F2**. (**A**) Pedigree of family F2. Individuals that were subjected to genetic screening are colored in red or green, respectively indicating whether the novel heterozygous **V16 variant** (chr6:99593030G>C) was present or not. (**B**) F2-III:1 and (**C**) F2-III:2. Fundus BE: symmetrical coloboma-like macular malformation indicative of grade 3 NCMD. BE: both eyes.

A

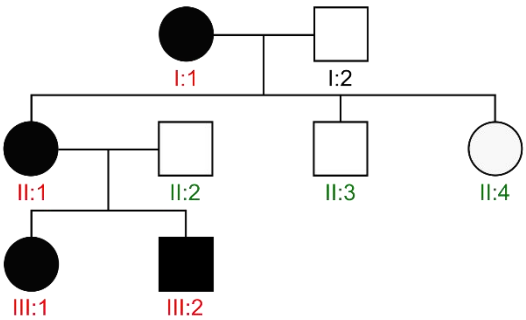

B

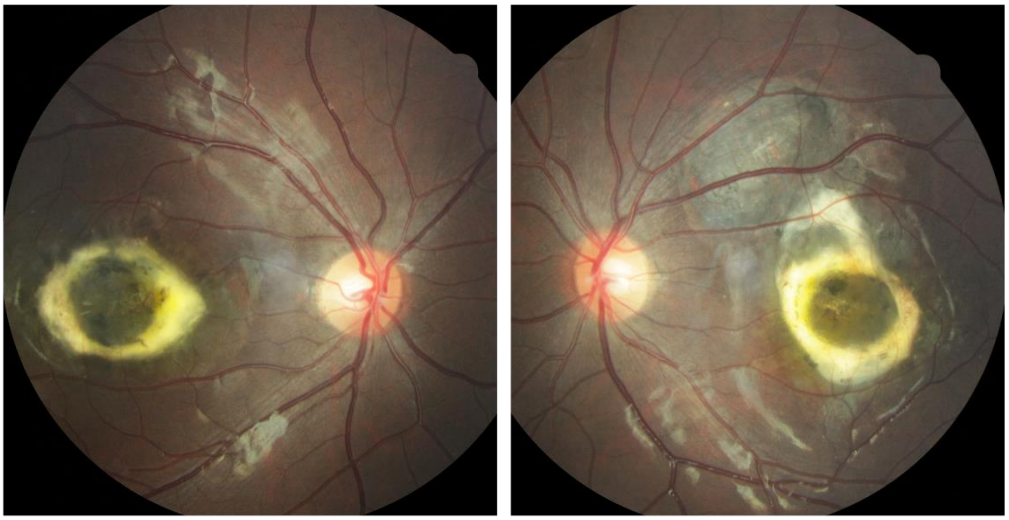

C

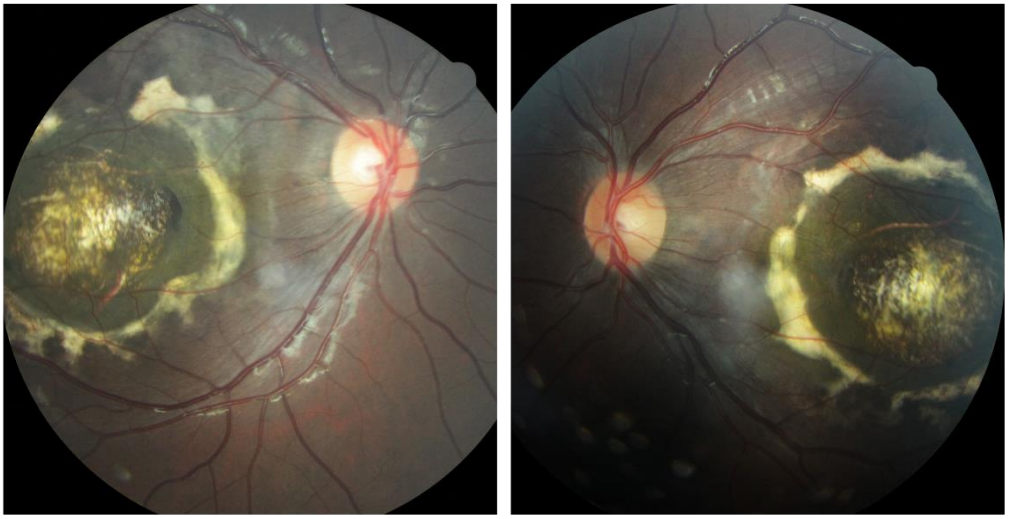

Suppl. Figure 8 - Overview of the genetic and clinical findings in **family F3**. (**A**) Pedigree of family F3. Individuals that were subjected to genetic screening are colored in red or green, respectively indicating whether the known heterozygous **V1 variant** (chr6:99593030G>T) was present or not. (**B**) F3-III:2. Multicolor (blue, green, and infrared) reflectance images BE: severe bilateral lesions of the RPE affecting the entire macular area, in accordance with grade 3 NCMD (**C**) F3-III:2. OCT LE: excavated lesion with a temporal shelving edge and subretinal fibrosis. (**D**) F3-II:1 and (**E**) F3-II:3. Fundus BE. Mild bilateral yellow specks in the central macula, compatible with grade 1 NCMD are indicated by an arrow. LE: left eye, RE: right eye, BE: both eyes.

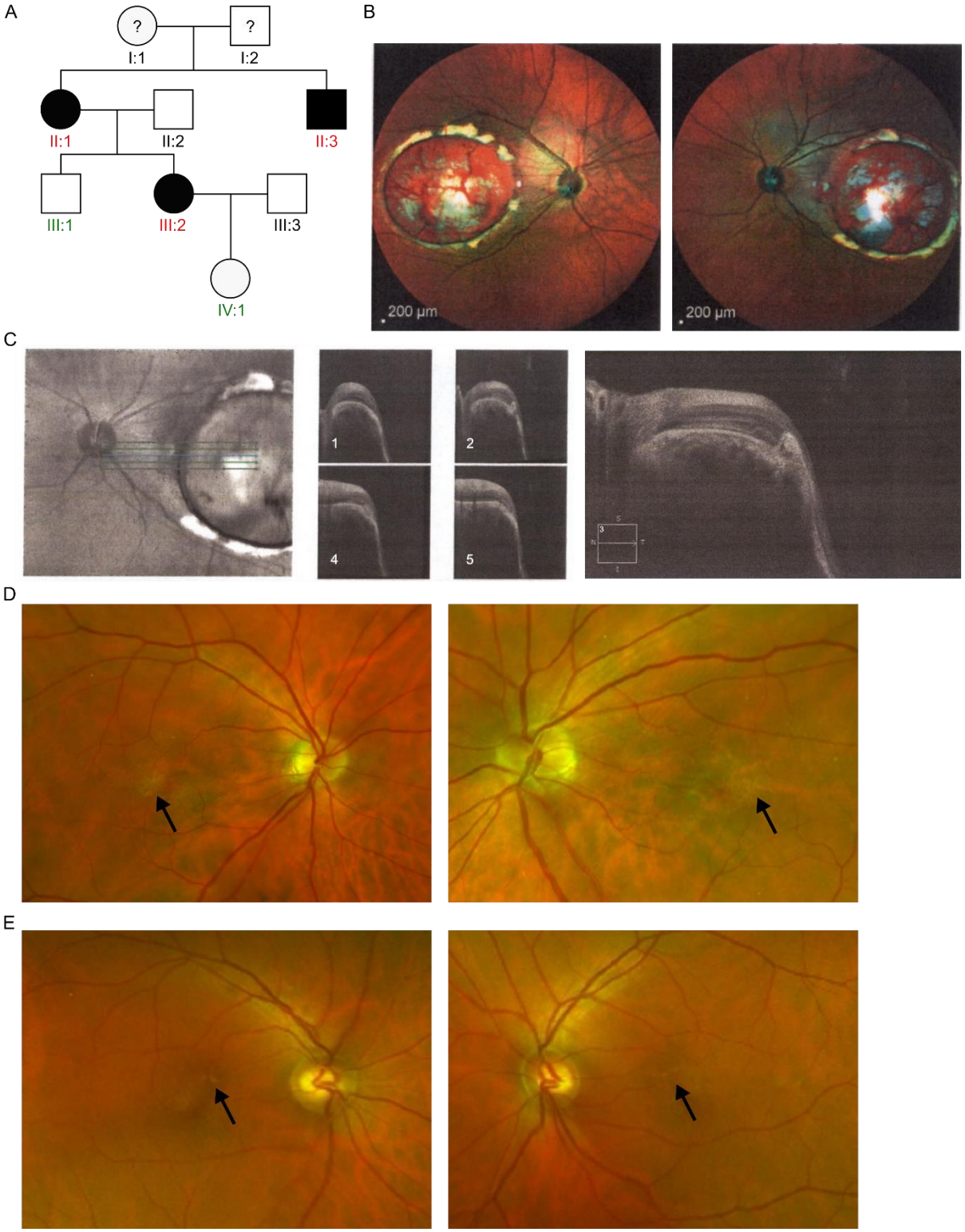

Suppl. Table 8 - Summary of genetic and clinical findings of the families with (likely) pathogenic variants. BCVA: best-corrected visual acuity, OCT: optical coherence tomography, RE: right eye, LE: left eye, ERG: electroretinogram, EOG: electrooculogram, Unk: unknown.

Family, pedigree number	Variant	Age/sex	BCVA	Fundus imaging	OCT	Other findings	NCMD grade
F1, III:1	V15	36/F	RE: 20/20 LE: 20/20	Yellowish-white lesions in the macula, encircled by hypopigmented halos and surrounded by hyperpigmentation	Focal RPE damage and focal neurosensory detachment	Normal color vision	2
F1, IV:1	V15	18/F	RE: 20/20 LE: 20/80	Circular plaques of coalescing yellowish-white masses in the macula and gross pigment deposits	Focal RPE damage, right focal neurosensory detachment and left submacular scarring	Normal color vision	2
F1, IV:2	V15	12/F	RE: 20/20 LE: 20/20	Mild RPE abnormalities with small macular drusen.	Mild RPE abnormalities with small macular drusen	Normal color vision	2
F1, II:3	V15	73/F	RE: 20/50 LE: 20/160	Chorioretinal macular atrophy with fibrotic changes more pronounced in the LE	Chorioretinal macular atrophy with fibrotic changes more pronounced in the LE, and vitreofoveal adhesion	-	3
F2, II:1	V16	41/F	RE: 20/30 LE: 20/40	Symmetrical elevated submacular yellow vitelliform-like lesions	Vitelliform lesions with central fibrosis	-	2
F2, III:1	V16	15/F	RE: 20/50 LE: 20/63	Symmetrical coloboma-like macular malformations	-	Flat/abnormal EOG, normal full-field ERG	3
F2, III:2	V16	12/M	RE: 20/70 LE: 20/80	Symmetrical coloboma-like macular malformations	-		3
F3, III:2	V1	37/F	RE: 20/200 LE: 20/200	Severe bilateral lesions of the RPE affecting the entire macular area	Excavated lesion with a temporal shelving edge and subretinal fibrosis	-	3
F3, II:1	V1	Unk/F	RE: 20/25 LE: 20/30	Yellow specks in the central macula of both eyes	-	-	1
F3, II:3	V1	Unk/M	RE: 20/30 LE: 20/25	Yellow specks in the central macula of both eyes	-	-	1

Suppl. Figure 9 - Visual representation of the results from the *in silico* SNV analysis using TRANSFAC. The A to C nucleotide change of the V10 variant causes the loss of an POU2F1 TFBS, while the A to G change of the V15 variant results in the gain of an HSF1 TFBS. The nucleotide changes are indicated by an arrow, both in the human DNA sequence and in the binding motif of the TFs.

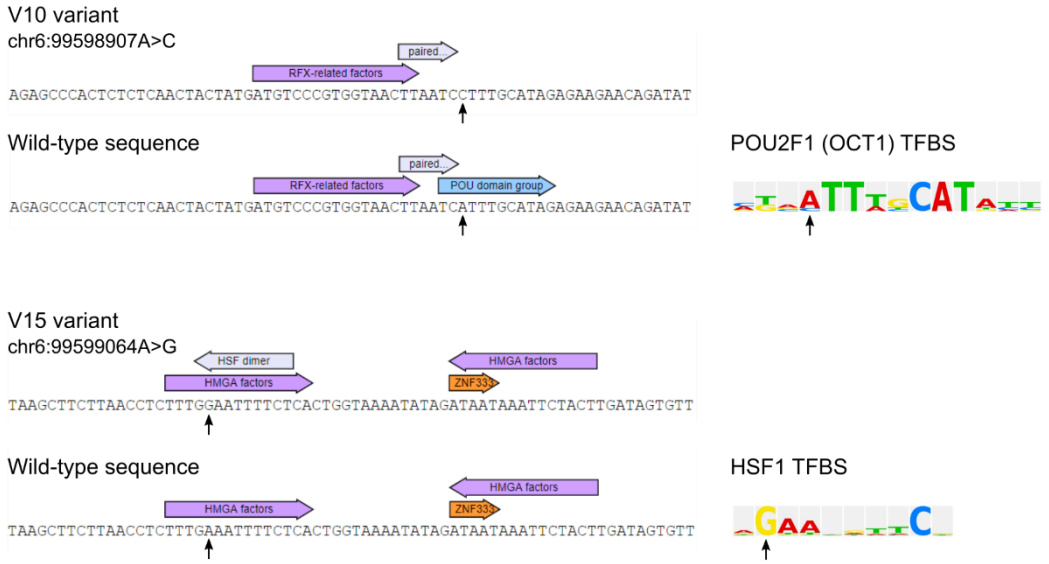

Suppl. Table 9 - Summary of the bioinformatics analyses of the eight previously reported NCMD-associated tandem duplications. For the breakpoint regions of each duplication, the degree of microhomology, the presence of repetitive elements, and the presence of sequence motifs, based on 40 previously described motifs (Fuzznuc) are indicated.

	V4	**V5**	**V6**	**V7**	**V8**	**V9**	**V13**	**V14**
Chr	6	5	6	6	5	5	6	6
Start (hg38)	99,572,329	3,587,787	99,548,350	99,536,433	4,391,264	4,396,814	99,484,588	99,560,265
End (hg38)	99,695,430	4,485,914	99,617,261	99,634,822	4,436,422	4,440,329	99,619,234	99,616,492
Inserted bases (bp)	22	15	5	0	0	0	0	0
Microhomology (bp)	0	2	0	2	2	2	3	3
5' breakpoint region								
Repetitive element	AluSx1	-	MER117	AluJb	-	-	AluJr	-
Number of sequence motifs	2	6	5	7	4	2	1	2
3' breakpoint region								
Repetitive element	L1M1	-	AluJo	L2a	L1M1	L1MC3	-	-
Number of sequence motifs	3	1	4	5	3	3	1	2
Conclusion								
Potential molecular mechanism	NHEJ	NHEJ	NHEJ	Replicative	Replicative	Replicative	Replicative	Replicative

Suppl. Figure 10 - Visualization of the joint point of the eight previously reported NCMD-associated tandem duplications. Inserted bases and microhomology are respectively indicated in pink and blue when present.

V4 (chr6:99572329-99695430)

```
5'    GAGTGCAATGGCTTCAGGCGATTCTCCTGCCTTAGC----------------------CTCCCAAGTAGCTGGGATTACAGGTGCCTGCCACCA
DUP   ATGTCAATGAAGAAATTAAGAAGGAAAAGTCAAAATATTTACTTTATGTGTTTGCATGCTCCCAAGTAGCTGGGATTACAGGTGCCTGCCACCA
3'    ATGTCAATGAAGAAATTAAGAAGGAAAAGTCAAAAT----------------------TTCTTGAAACAAATGATAATGGAAACACAACATACC
```

V5 (chr5:3587787-4485914)

```
5'    GGGGGTTTGGGAAGGGCATCTGGAGGAATGCAGAGGA---------------GACTGAGAAGAGGAACTTCCCGATCTGGGGATTTTGC
DUP   TACATCAATACCATATGCAAAATTTAATTCATAATGACTGAGAATTCATAATGACTGAGAAGAGGAACTTCCCGATCTGGGGATTTTGC
3'    TACATCAATACCATATGCAAAATTTAATTCATAATGA---------------GAATCATCAGACATAAATGTTAGCTTAAAACTATAAA
```

V6 (chr6:99548350-99617261)

```
5'    CACTGGGTAGGACACCACTCAAAATCCTTTCAAATC-----CAGTCCTTTCAGGGAACTGCCAGTAATACAGAAGTG
DUP   CTCATGTCTGTAGTTTCAGCAACTCAGGAGGCTGAGTCCTGCAGTCCTTTCAGGGAACTGCCAGTAATACAGAAGTG
3'    CTCATGTCTGTAGTTTCAGCAACTCAGGAGGCTGAG-----GCAGAAGGCTAGCTTAAGCCCAGGAATTCAAGGCTG
```

V7 (chr6:99536433-99634822)

```
5'    TTATACAACAGTCTTTTTTTTTTTTTTTTTAAGACAGGGTCTCACTCTGTCTCCTGGCTGGAGTGCAGTGGC
DUP   AGGAGAAGGAAAGAGATGAATCAGTGTTGATTTCTAGGGTCTCACTCTGTCTCCTGGCTGGAGTGCAGTGGC
3'    AGGAGAAGGAAAGAGATGAATCAGTGTTGATTTCTAGATTTTAGGCTTGCAAACTGGGTGGCTGGTGGTGGT
```

V8 (chr5:4391264-4436422)

```
5'    TGTGGCCCTTTCTTTACATTACTGTGGTATCAGTTGTAATGTCTCTCATTTATATTATATTATATTATATAC
DUP   ACTGATGACTTATAAAGTTCATTTGGTGTGGTCATGTAATGTCTCTCATTTATATTATATTATATTATATAC
3'    ACTGATGACTTATAAAGTTCATTTGGTGTGGTCATGTTTTCTCGAATAGTCTTGATGCTTGTGAATATTCTT
```

V9 (chr5:4396814-4440329)

```
5'    TTTTTGGTAGTGAACAAAGCCAAGTAAACACAATAAAGAAAATCAGCCAATGATAGCTAAGAGTGGAGATGA
DUP   TAATATAAAGGAAGCATCCATGAGTTGATACTGGTAAGAAAATCAGCCAATGATAGCTAAGAGTGGAGATGA
3'    TAATATAAAGGAAGCATCCATGAGTTGATACTGGTAAAATAAATGATTGAATGGTGGAATAGATGGATCTCC
```

V13 (chr6:99484588-99619234)

```
5'    ACACTTTGGGAGGCCAAGGTGGAAGGATCACTTGAGCCCAGAGTGGAAGGCCCGCTTGGGCAACATAGGGAG
DUP   GGAGGGGAGCTGCGGCACCCGCGCCGTGCGCTCTCGCCCAGAGTGGAAGGCCCGCTTGGGCAACATAGGGAG
3'    GGAGGGGAGCTGCGGCACCCGCGCCGTGCGCTCTCGCCATCTGCCGCCTTCCCAACGGGAAGAGGGCAGAGG
```

V14 (chr6:99560265-99616492)

```
5'    TAATATTTAAATAAAATCAAATATTACATAGAATTATTAGAATTAGAAAACTCAATCCATAATAAGGACCTT
DUP   GTTAAAAATGCCCATTATTTTCTGAATCCTGAATGATTAGAATTAGAAAACTCAATCCATAATAAGGACCTT
3'    GTTAAAAATGCCCATTATTTTCTGAATCCTGAATGATTTGCAAGTCTTCACCTTTCTTCCTGTTGGCAACAC
```

Suppl. Table 10 - Results from the luciferase assays for the known and novel SNVs, the three artificial tandem duplications, and the set of fourteen non-coding regions of interest. For each assay, the fold change of the luciferase reporter level relative to the level of the reference control luciferase vector is given. For the variants, the P-values were obtained by likelihood ratio tests of the linear mixed effects model with the fixed effect against a null model without this effect. cCRE: candidate CRE, MHS: mutational hotspot, pos: positive, NS: not significant, neg: negative.

Insert	Effect	Fold change	P-value
Known & novel SNVs (MHS1)			
V1	pos	2.58 ± 0.27	2.4E-05
V2	pos	2.75 ± 0.21	2.6E-07
V3	pos	1.62 ± 0.15	5.1E-04
V12	pos	2.03 ± 0.13	6.0E-07
V16	pos	3.24 ± 0.19	1.9E-09
Known & novel SNVs (MHS2)			
V10	neg	0.59 ± 0.07	1.2E-05
V11	neg	0.70 ± 0.07	3.5E-04
V15	neg	0.64 ± 0.07	8.1E-05
Tandem duplications			
MHS1dup	neg	0.53 ± 0.03	5.7E-12
cCRE1dup	neg	0.52 ± 0.03	2.1E-12
SDRdup	neg	0.46 ± 0.04	6.6E-11
Non-coding region of interest			
MHS1	pos	1.90 ± 0.08	6.2E-09
MHS2 = cCRE4	NS	0.88 ± 0.07	8.0E-02
cCRE1	NS	1.02 ± 0.07	8.1E-01
cCRE5	pos	2.57 ± 0.08	6.7E-13
cCRE7	NS	0.98 ± 0.08	8.2E-01
cCRE8	pos	3.04 ± 0.10	6.2E-14
cCRE9	pos	2.07 ± 0.08	1.6E-10
cCRE10	pos	1.38 ± 0.08	2.1E-04
cCRE11	neg	0.62 ± 0.06	2.1E-05
cCRE12	neg	0.49 ± 0.07	1.1E-06
cCRE13	NS	0.96 ± 0.08	6.4E-01
cCRE14	pos	6.82 ± 0.32	1.2E-12
cCRE15	pos	2.44 ± 0.15	2.2E-08
SDR	NS	1.12 ± 0.06	6.1E-02

Suppl. Figure 11 - Results from the luciferase assays for the set of fourteen cCREs. The bar plot shows, for each cCRE, the fold change of the luciferase reporter level relative to the level of the negative control luciferase vector (fold change = 1). cCRE: candidate CRE, MHS: mutational hotspot, SDR: shared duplicated region, neg: negative, NS: not significant, pos: positive, ***: P<0.001.

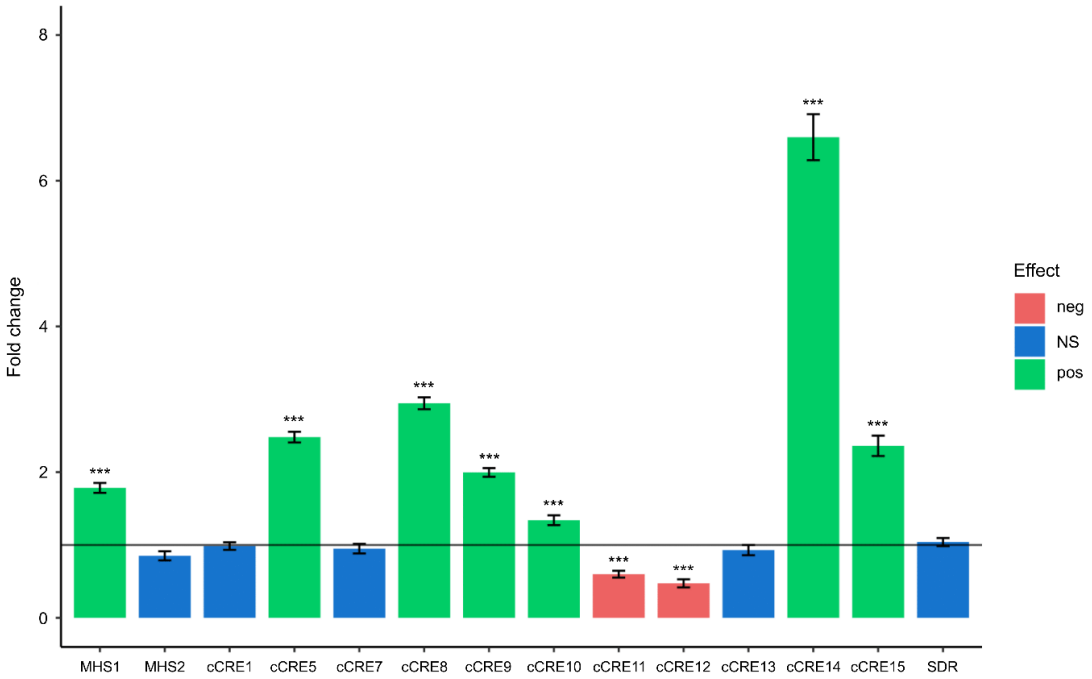

Suppl. Table 11 - Summary of the results from the *in vivo* transgenic enhancer assays in *Xenopus tropicalis* and albino *Xenopus laevis* using a fluorescent enhancer detection vector and transgenesis via I-*Sce*I meganuclease. For each of the five non-coding regions of interest, it is indicated where EGFP reporter expression was observed at five different developmental stages. NC: neural crest, NE: no expression, NDA: no data available.

Region	Species	NF stage 15	NF stage 20	NF stage 42/43	NF stage 45	NF stage 55
cCRE14	*X. tropicalis*	Neural plate	Neural tube	NC derivatives, eye	NC derivatives, eye	Eye
	X. laevis	NE	NE	NC derivatives, eye, brain	NDA	NDA
SDR	*X. tropicalis*	NE	NE	NDA	NDA	Eye
	X. laevis	NE	NE	Eye, brain	NDA	NDA
MHS1	*X. tropicalis*	NDA	NDA	NDA	NDA	NDA
	X. laevis	NE	NE	NE	NE	NE
MHS2	*X. tropicalis*	NE	NE	Eye	Eye	NDA
	X. laevis	NE	NE	Eye, brain	NDA	NDA
cCRE1	*X. tropicalis*	NE	NE	Eye	NDA	NDA
	X. laevis	NE	NE	Eye, brain	NDA	NDA

Suppl. Figure 12 - Comparison of the seven cCREs we identified in the *PRDM13* locus using UMI-4C profiling integrated into our retina-specific multi-omics database RegRet (black bars) with the ten macula-specific CREs identified by Green *et al.* (2021) using the activity-by-contact (ABC) method (grey bars).[80]

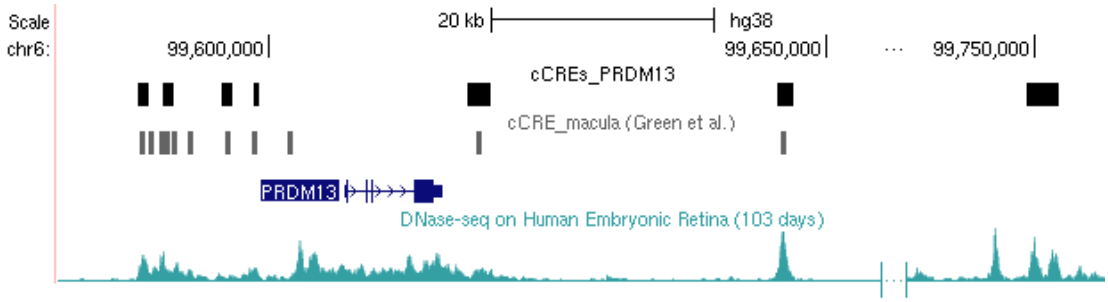

Data availability

All unique materials and data that support the findings of this study are readily available from the corresponding author upon request or from standard commercial sources (as listed in the methods).

Acknowledgements

This work was supported by grants from Ghent University Special Research Fund (BOF20/GOA/023) (EDB, KV, BPL); Ghent University Hospital Innovation Fund NucleUZ (EDB); JED Foundation (EDB); H2020 Marie Sklodowska-Curie Innovative Training Networks (ITN) StarT (grant No. 813490) (EDB, KV, JLGS, JJT, JRM); EJP RD Solve-RET EJPRD19-234 (EDB, PL, BK, CR, JLGS, JJT, JRM), SNSF grant # 204285 (CR), Foundation Fighting Blindness in Columbia, MD (Grant #: BR-GE-1216-0715-CSH). SVS (1145719N) is PhD fellow of the Research Foundation-Flanders (FWO), EDB (1802220N) and BPL (1803816N) are FWO Senior Clinical Investigators; MBS, VLS and ADR are Early Starting Researcher of ITN StarT (grant No. 813490). BK, BPL, CJFB, EDB, PL and VV are members of ERN-EYE (Framework Partnership Agreement No 739534-ERN-EYE). An unrestricted grant from The Molecular Insight Research Foundation (KWS)

Author contributions

SVS: Conception and project design, acquisition of data, analysis and interpretation of data, drafting and revising the manuscript.

KWS: Acquisition of data, analysis and interpretation of data, drafting and revising the manuscript.

MBC: Project design, acquisition of data, analysis and interpretation of data, drafting and revising the manuscript.

VLS: Project design, acquisition of data, analysis and interpretation of data, drafting and revising the manuscript.

ED: Project design, acquisition of data, analysis and interpretation of data, revising the manuscript.

FSS: Acquisition of data, analysis and interpretation of data, revising the manuscript.

SA: Acquisition of data, analysis and interpretation of data, revising the manuscript.

TVDS: Acquisition of data, analysis and interpretation of data, revising the manuscript.

ADR: Acquisition of data, analysis and interpretation of data, revising the manuscript.

TR: Acquisition of data, revising the manuscript.

MVH: Acquisition of data, revising the manuscript.

SV: Analysis and interpretation of data, revising the manuscript.

IB: Acquisition of data, revising the manuscript.

AAB: Acquisition of data, revising the manuscript.

CJFB: Acquisition of data, revising the manuscript.

JDZ: Acquisition of data, revising the manuscript.

CFI: Acquisition of data, revising the manuscript.

BK: Acquisition of data, revising the manuscript

VV: Acquisition of data, revising the manuscript

BPL: Acquisition of data, revising the manuscript.

CR: Acquisition of data, revising the manuscript.

JvdE: Acquisition of data, revising the manuscript.

MJvS: Acquisition of data, revising the manuscript.

VV: Acquisition of data, revising the manuscript.

JLGS†: Project design, acquisition of data, analysis and interpretation of data.

JJT: Project design, acquisition of data, analysis and interpretation of data, revising the manuscript.

JRMM: Project design, acquisition of data, analysis and interpretation of data, revising the manuscript.

PL: Acquisition of data, analysis and interpretation of data, drafting and revising the manuscript.

KV: Project design, acquisition of data, analysis and interpretation of data, revising the manuscript.

EDB: Conception and project supervision, acquisition of data, analysis and interpretation of data, drafting and revising the manuscript.

Competing interests

The authors declare no competing interests.